ADVANCED ENERGY MATERIALS
www.advenergymat.de

Vanadyl Phosphates A_xVOPO_4 (A = Li, Na, K) as Multielectron Cathodes for Alkali-Ion Batteries

*Natasha A. Chernova, Marc Francis V. Hidalgo, Carol Kaplan, Krystal Lee, Isiksu Buyuker, Carrie Siu, Bohua Wen, Jia Ding, Mateusz Zuba, Kamila M. Wiaderek, Ieuan D. Seymour, Sylvia Britto, Louis F. J. Piper, Shyue Ping Ong, Karena W. Chapman, Clare P. Grey, and M. Stanley Whittingham**

Vanadyl phosphates comprise a class of multielectron cathode materials capable of cycling two Li^+, about 1.66 Na^+, and some K^+ ions per redox center. In this review, structures, thermodynamic stabilities, and ion diffusion kinetics of various A_xVOPO_4 (A = Li, Na, K, NH_4) polymorphs are discussed. Both the experimental data and first-principle calculations indicate kinetic limitations for alkali metal ions cycling, especially between for $0 \le x \le 1$, and metastability of phases with $x > 1$. This creates challenges for multiple-ion cycling, as the slow kinetics call for nanosized particles, which being metastable and reactive with organic electrolytes are prone to side reactions. Thus, various synthesis approaches, surface coating, and transition metal ion substitution strategies are discussed here as possible ways to stabilize A_xVOPO_4 structures and improve alkali metal ion diffusion. The role of advanced characterization techniques, such as X-ray absorption spectroscopy, diffraction, pair distribution function analysis and ^7Li and ^{31}P NMR, in understanding the reaction mechanism from both structural and electronic points of view is emphasized.

1. Introduction

Vanadium-based compounds have long been researched as cathode materials for Li-ion batteries due to their ability to cycle more than one Li ion per vanadium redox center.[1] Moreover, multiple V oxidation states contribute to the outstanding structural diversity of vanadium compounds with a variety of open structures providing facile pathways for Li diffusion.[2] Vanadium oxides and related vanadium oxide nanostructures have been recently reviewed,[3] as were the polyanionic vanadium compounds, where higher voltage for Li intercalation is achieved due to the inductive effect of polyanions, which also increases the structural stability.[1a,b,4] This review will focus on vanadyl phosphates due to their high theoretical capacity for Li intercalation, 305 mAh g^{-1} (based on Li_2VOPO_4 molecular weight), coming from two redox processes: V^{4+}/V^{5+} occurring at 3.9 V and V^{4+}/V^{3+} on average at 2.25 V. This results in a high energy density of about 980 Wh kg^{-1}, exceeding that of NASICON phases of $Li_3V_2(PO_4)_3$, and most of the vanadium oxides (Table SI, Supporting Information). The polyanionic framework of (Li)$VOPO_4$ ensures better thermal stability than that of layered oxides.[5] The challenges of (Li)$VOPO_4$ compounds as cathodes for alkali metal cation cycling in secondary batteries comes from their structural diversity and reactivity, combined with low ionic and electronic conductivities.

Dr. N. A. Chernova, Dr. M. F. V. Hidalgo, C. Kaplan, K. Lee, I. Buyuker, Dr. C. Siu, Prof. J. Ding, Prof. M. S. Whittingham
NorthEast Center for Chemical Energy Storage
Binghamton University
Binghamton, NY 139020-6000, USA
E-mail: stanwhit@binghamton.edu

Dr. B. Wen
Department of Materials Science and Engineering
Massachusetts Institute of Technology
Cambridge, MA 02139, USA

Dr. M. Zuba, Prof. L. F. J. Piper
Department of Physics
Applied Physics and Astronomy and NorthEast Center for Chemical Energy Storage
Binghamton University
Binghamton, NY, USA

Dr. K. M. Wiaderek
X-ray Science Division
Advanced Photon Source
Argonne National Laboratory
Argonne, IL 60439, USA

Dr. I. D. Seymour, Dr. S. Britto, Prof. C. P. Grey
Department of Chemistry
University of Cambridge
Lensfield Road, Cambridge CB2 1EW, UK

Prof. S. P. Ong
Department of NanoEngineering
University of California San Diego
9500 GilmanDrive #0448, La Jolla, CA 92093, USA

Prof. K. W. Chapman
Department of Chemistry
Stony Brook University
Stony Brook
New York, NY 11974, USA

The ORCID identification number(s) for the author(s) of this article can be found under https://doi.org/10.1002/aenm.202002638.

DOI: 10.1002/aenm.202002638

In this review, we will summarize available data on relative stabilities of (Li)$VOPO_4$ polymorphs, their synthesis methods in relation to electrochemical performance enhancement, reaction mechanism in Li-ion batteries, the role of surface coating and substitution in surface stabilization and kinetics improvement. We will base this work on excellent reviews of polyanion compounds by Masquelier and Croguennec[1b] (2013) and Whittingham,[1a] (2014) and cover the most recent progress, concluding with the remaining challenges and future research directions.

2. Li_xVOPO_4 (x = 0, 1) Polymorphism and Stability

Vanadyl phosphate, $VOPO_4$, is found in at least seven different crystallographic forms varying from layered structures to 3D lattices (**Figure 1**).[6] For $LiVOPO_4$, only three stable polymorphs exist, corresponding to α_1, β, and ε-$VOPO_4$ phases.[7] Here the lithiated phases are named by the prefixes of their $VOPO_4$ parent phases to avoid confusion, as was introduced in the previous review.[1a] Since stable electrochemical performance is directly related to the phase stability, the further focus will be on these three phases, which all contain VO_6 octahedra with a short vanadyl V=O bond (1.6–1.8 Å), and a long V—O bond, around 2.2 Å, connected by PO_4 tetrahedra. For ε-$VOPO_4$, two structures were reported in the literature with space groups $P2_1/n$[6d,8] and Cc.[9] The difference between the two is in the orientation of the VO_5 pyramids (long V—O bond omitted), which all point in the same direction in the Cc structure and alternate in P21/n. Density functional theory (DFT) calculations and the goodness of the Rietveld refinements both point toward the Cc structure being more stable and better fitting the experimental X-ray diffraction (XRD) patterns.[9,10] Upon lithiation of ε-$VOPO_4$, the triclinic form of ε-$LiVOPO_4$ is formed.[8a] Its connectivity is essentially the same as in ε-$VOPO_4$, but VO_6 octahedra are tilted, and correspondingly, the PO_4 tetrahedra are tilted too. Li ions occupy two distorted five-coordinated sites in tunnels along the [110] direction in the structure. In both compounds, long and short V—O bonds alternate along the chain. The calculations of V_{Li+} migration barriers in ε-$LiVOPO_4$ indicate two pathways A→B→C with lower barriers of 244 meV formed by Li1 sites and D→E→F with higher barriers (703 meV) formed by Li2 sites (Figure 1). At the beginning of discharge, there are three distinct paths for A^+ diffusion in ε-$VOPO_4$. For paths A→B, A→C, and A→D, the barriers for Li^+ migrations are 271, 629, and 637 meV, respectively, and those for Na^+ migrations are 516, 674, and 694 meV, respectively (Figure 1).[11] The kinetic limitations to the 1st Li^+ intercalation into ε-$VOPO_4$ were demonstrated by Quackenbush et al. using a combination of soft and hard X-ray photoelectron spectroscopy. It was shown that due to slow Li intercalation kinetics, the second Li starts to intercalate before the intercalation of the first Li is complete, creating a Li concentration gradient within ε-$VOPO_4$ nanoparticles.[12] We will show later, that even in the optimized nanocrystalline ε-$VOPO_4$/graphene material, the rate performance is limited by the slower high-voltage process, which remains one of the major limitations of this material.[13]

Closely related to ε-$VOPO_4$ is β-$VOPO_4$ which adopts an orthorhombic structure. These two structures have essentially the same VO_6 connectivity along the chains, with the exception of the tilting of VO_6 octahedra. The oxygen atoms in the direction of the VO_6 chains are crystallographically equivalent in the β-structure, while in ε-structure they are different. However, the chains are connected differently by PO_4 tetrahedra in ε- and β-structures. In ε-$VOPO_4$, PO_4 tetrahedra alternate between "up" and "down," while in β-$VOPO_4$ the PO_4 tetrahedra are all "up" in one row and all "down" in the next one (Figure 1). Thus, the transition between ε- and β-phases involves a switch of half of the P atoms from "up" to "down" position. According to the DFT calculations, β-$VOPO_4$ is more stable than ε-$VOPO_4$,[11,14] which agrees well with experimentally observed transformation from ε-$VOPO_4$ to β-$VOPO_4$ at 700 °C.[6d] The orthorhombic structure is preserved in the β-$LiVOPO_4$ phase, where the Li ions are located in octahedral sites that share two faces with VO_6 octahedra and form 1D diffusion channels along the [010] direction. DFT calculations disagree on which of the ε- and β-$LiVOPO_4$ phases is more stable,[11,14] they both do show that

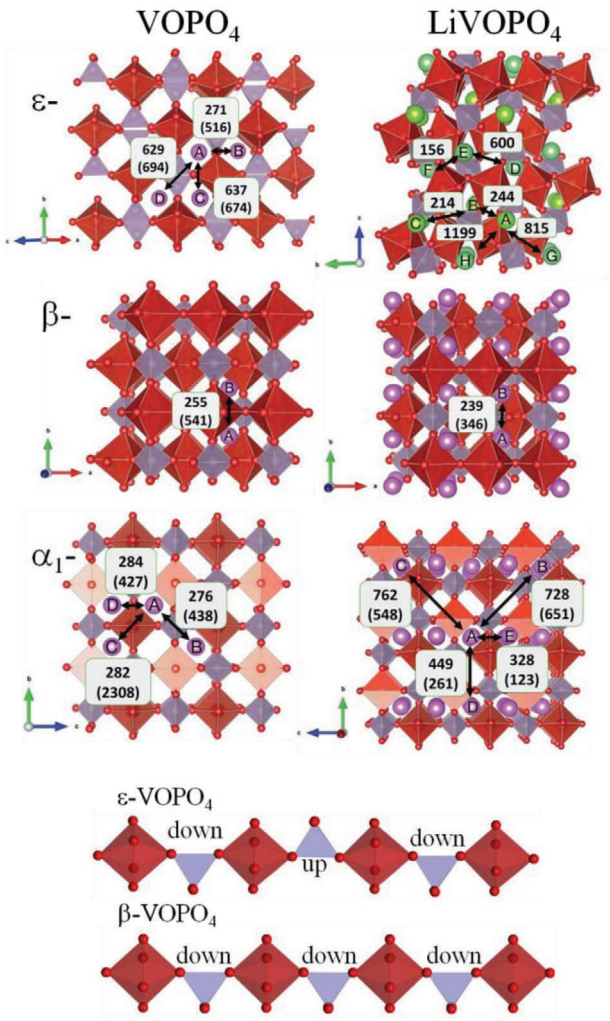

Figure 1. Crystal structures of ε-, β-, α_1-$VOPO_4$, and $LiVOPO_4$ phases along with VO_6 and PO_4 connectivity comparison between ε and β phases. The numbers indicate Li^+ and (Na^+) diffusion barriers (meV) in $VOPO_4$ and corresponding vacancy diffusion barriers in $LiVOPO_4$. Reproduced with permission.[11] Copyright 2017, The Royal Society of Chemistry.

the stability differences between these phases are small, suggesting that other factors during the synthesis may play more significant roles in determining which phase forms.

There is only one symmetrically distinct v_{A+} diffusion path in β-$AVOPO_4$, which is denoted as path A→B along the [010] direction (Figure 1). The calculations show that the barriers of v_{Li+} and v_{Na+} migrations in β-$LiVOPO_4$ and β-$NaVOPO_4$ are 239 and 255 meV, respectively, and the barriers of Li^+ and Na^+ migration in β-$VOPO_4$ are 346 and 541 meV, respectively. For β-A_xVOPO_4 (x = 0, 1), both Li^+ and Na^+ exhibit 1D diffusion along the [010] direction, in line with the previous simulation and experimental results.[14,15]

Hameed et al. first showed that $LiVOPO_4 \cdot 2H_2O$ can be heated to form the metastable α_I-$LiVOPO_4$ (Figure 1) via a dehydration step and a slight shift in the $VOPO_4$ layer.[16] The layered α_I-$LiVOPO_4$ structure has four Li^+ diffusion pathways, all with migration barriers significantly higher than in ε- and β-$LiVOPO_4$. In contrast, the migration barriers for Na^+ ion diffusion are the lowest.[11] It is consistent with the electrochemical performance of α_I-phase in Li- and Na-ion cells, as will be discussed later.

Hameed et al. also demonstrated that heating the $LiVOPO_4 \cdot 2H_2O$ at higher temperatures can yield ε-$LiVOPO_4$. Hidalgo et al. built on this study by utilizing $LiVOPO_4 \cdot 2H_2O$ as a precursor to experimentally study the thermodynamic stabilities of all three $LiVOPO_4$ polymorphs.[17] This study is based upon the idea that by starting with the same metastable precursor and heating it to allow the crystal structure to reorganize into a more stable conformation, the thermodynamic stabilities of each polymorph can be directly compared. Also, by utilizing the same precursor, biases induced by the different synthesis methods can also be removed, which is key for differentiating the thermodynamically similar β and ε polymorphs.

As shown using in situ variable temperature XRD (**Figure 2**a) heating $LiVOPO_4 \cdot 2H_2O$ in an inert atmosphere results in the following transition: $LiVOPO_4 \cdot 2H_2O \rightarrow \alpha_I \rightarrow \beta + \varepsilon \rightarrow \varepsilon$. As expected from the metastable nature of α_I phase, confirmed by the DFT calculations,[11,14] the $\alpha_I \rightarrow \beta + \varepsilon$ transition is not reversible, while the $\beta \leftrightarrow \varepsilon$ transition is reversible.[17] The equal ratio of the β and ε polymorphs confirm the calculations that both polymorphs have similar thermodynamic stabilities.

If the in situ XRD with heating experiment was repeated in O_2, as shown in Figure 2b, the transitions observed are: $LiVOPO_4 \cdot 2H_2O \rightarrow \alpha_I + \beta \rightarrow \beta \rightarrow$ amorphous melt + ε. This suggests that β-$LiVOPO_4$ is O-rich, while ε-$LiVOPO_4$ is O-poor. The DFT calculations (Figure 2d) show that ε-$LiVOPO_4$ is always more stable than β-$LiVOPO_4$ if O-vacancies are present, and that β-$LiVOPO_4$ is more stable if these vacancies are absent. This was also confirmed by thermogravimetric analysis with mass spectroscopy (TGA-MS) experiments showing that O_2 is released during the $\beta \rightarrow \varepsilon$ transition. This explains why the $\beta \rightarrow \varepsilon$ transition occurs at higher temperatures, as those are needed for O-loss to occur. Conversely, the $\varepsilon \rightarrow \beta$ transition can occur by heating ε-$LiVOPO_4$ in O_2 in order to fill the O-vacancies.

3. Metastable Structures of Li_xVOPO_4 (x = 1.5, 1.75, 2) Phases: NMR Insight

A_xVOPO_4 phases with $x > 1$ can only be obtained by chemical or electrochemical intercalation of A^+ ions into corresponding

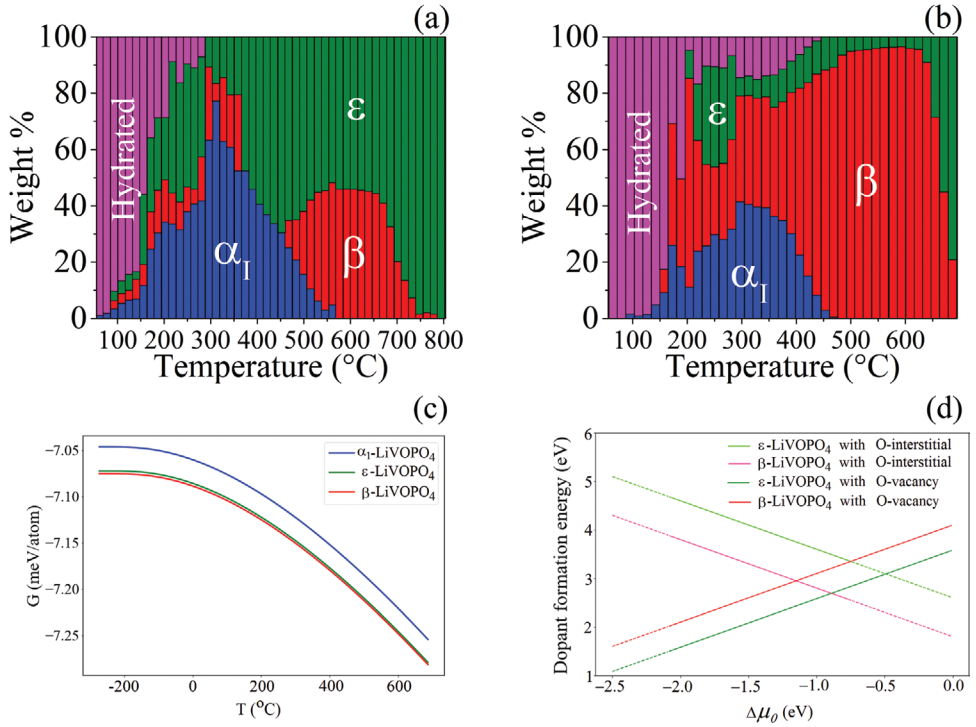

Figure 2. In situ XRD with heating showing the general transition from $\alpha_I \rightarrow \beta \rightarrow \varepsilon$ with increasing temperature in a) Ar and b) O_2. These are explained using c) Gibbs free energy diagrams at various temperatures of each polymorph, and d) energy above hull calculations of β- and ε-$LiVOPO_4$ with O-defects. Reproduced with permission.[17] Copyright 2019, The Royal Society of Chemistry.

$VOPO_4$ or $AVOPO_4$ phases.[10a,18] Bianchini et al. first reported intermediate $Li_{1.5}VOPO_4$, $Li_{1.75}VOPO_4$ phases formed upon electrochemical lithiation of ε-$LiVOPO_4$ and characterized the structure of ε-Li_2VOPO_4 obtained by chemical lithiation of ε-$LiVOPO_4$ using X-ray and neutron diffraction data.[10a] ε-Li_2VOPO_4 preserves the ε-$VOPO_4$ network of VO_6 octahedra and PO_4 tetrahedra, however, upon reduction of vanadium to 3+, VO_6 octahedra become more symmetrical without short vanadyl and long opposite V—O bonds. This leads to overall shortening of VO_6 chains as evidenced by a decrease in *b*-lattice parameter. Lin et al. proposed structures of ε-$Li_{1.5}VOPO_4$ and $Li_{1.75}VOPO_4$ phases using DFT calculations.[19] The predicted $Li_{1.5}VOPO_4$ and $Li_{1.75}VOPO_4$ structures have $P\bar{1}$ symmetry, in agreement with the experimental data.[10a,18a,19] The lowest energy $Li_{1.75}VOPO_4$ structure is a supercell that is twice the size of the primitive cell of Li_2VOPO_4. It is proposed that Li disorder is likely present in $Li_{1.75}VOPO_4$ given the presence of multiple orderings that are close in energy (and hence, potentially thermodynamically accessible at finite temperatures) to the ground-state ordering. It is consistent with experimental observations by Harrison[18a] and Bianchini.[10a] It should be noticed that both Bianchini's and Lin's works used $LiVOPO_4$ synthesized by solid-state method and subjected to high-energy ball-milling to reduce particle size, which introduces structural disorder as will be discussed later.[20] Wangoh et al., using a combination of hard and soft X-ray photoelectron and absorption spectroscopy techniques, have shown that uniform Li distribution in ε-$LiVOPO_4$ is a prerequisite to the formation of $Li_{1.5}$ and $Li_{1.75}VOPO_4$ phases. Also, it ensures uniform second Li intercalation to form the Li_2VOPO_4.[21] Further insights into the Li_2VOPO_4 structure were obtained using nanocrystalline ε-$VOPO_4$ as a starting material.[13,22] In the paper by Siu et al.[13] we have shown that two Li can be intercalated into ε-$VOPO_4$ by comparison of ^{7}Li NMR spectra obtained by chemical and electrochemical lithiation. A chemically lithiated ε-Li_2VOPO_4 sample was previously investigated by Davis et al. using ^{6}Li exchange NMR in which three distinct Li environments were found to be present.[23] Li sites in ε-Li_2VOPO_4 were assigned by Seymour et al.[22] based on ^{7}Li and ^{31}P NMR data. In addition to ε-Li_2VOPO_4 structure proposed by Bianchini,[10a] where Li ions are located in two distinct tunnels along the [110] direction: tunnel 1 containing 2 × Li(1a), 2 × Li(2), and 1 × Li(3) sites and tunnel 2 containing 2 × Li(1a) and 1 × Li(3) (**Figure 3**), structures with just one Li tunnel containing Li(1a), Li(1b), Li(2), and Li(3) sites were enumerated and optimized. The lowest energy single tunnel structure (Figure 3a) was found lower in energy than the double-tunnel structure (Figure 3b). Also, ^{7}Li and ^{31}P NMR shifts calculated for the lowest energy single tunnel structure were found to match the experimentally observed shifts. Moreover, the single tunnel structure also produced a better fit to X-ray diffraction and pair-distribution function (PDF) data of ε-Li_2VOPO_4. It should be noted that the single-tunnel structure is predicted to be only slightly lower in energy that the one proposed by Bianchini et al. Thus, in more disordered samples produced from ε-$LiVOPO_4$ subjected to high-energy ball-milling the double-tunnel structure may also exist.

In contrast with more studied ε-$LiVOPO_4$, much less is known about the mechanism of lithiation of the β phase. Ren et al.[24] have demonstrated the use of β-$LiVOPO_4$ as an anode in lithium-ion batteries and suggested that one Li ion per formula unit can be intercalated into the structure to give Li_2VOPO_4, with deeper discharge down to 0.01 V resulting in the formation of metallic vanadium and Li_3PO_4. Allen et al.[18b] have investigated the electrochemical performance of both ε- and β-$LiVOPO_4$ and the evolution of the local geometry of the VO_6 octahedra with electrochemical cycling using X-ray absorption spectroscopy (XAS). Harrison et al.[18a] studied the phases formed on electrochemical and chemical lithiation of ε- and β-$LiVOPO_4$ using mainly X-ray and neutron diffraction as well as X-ray spectroscopy methods. They suggest a two-phase mechanism operating upon lithiation of β-$LiVOPO_4$, with the plateau in the galvanostatic charge curve at 2 V arising due to equilibrium between a two-phase mixture of β-$LiVOPO_4$ andβ-Li_2VOPO_4. Lin et al. predicted using DFT calculations an existence of an intermediate metastable $Li_{1.5}VOPO_4$ phase and β-Li_2VOPO_4.[11] Britto et al. build on this work by optimizing the lowest energy structures on the convex hull for $x = 1$, 1.5, and 2 in β-Li_xVOPO_4, calculating NMR shifts and comparing them to the experimentally observed shifts in β-Li_xVOPO_4 synthesized by chemical and electrochemical lithiation of β-$LiVOPO_4$ and β-$VOPO_4$.[25] This work shows that β-$LiVOPO_4$ has close to zero ^{7}Li NMR shift, which is unusual for a paramagnetic compound and results from a superposition of bond pathways with positive and negative shifts. Upon electrochemical insertion of 0.5Li into β-$LiVOPO_4$ new resonances arise at 46 and 264 ppm indicative of Li intercalation into disordered tetrahedral sites (Li2 and Li5 in **Figure 4**). DFT calculations suggest that the ^{7}Li shifts close to 50 ppm arise from local environments in β- $Li_{1.5}VOPO_4$, while the negative shifts and those >200 ppm are due to octahedral and (highly) distorted "tetrahedral" environments, respectively, in β- Li_2VOPO_4. Interestingly, this 50 ppm shift does not appear in chemically lithiated Li_2VOPO_4 sample, and it disappears upon sample storage. It is consistent with a metastable nature of β-$Li_{1.5}VOPO_4$ predicted by DFT calculations.

It should be noted that the observed NMR shifts of electrochemically obtained β-Li_xVOPO_4 could not be explained by one single composition or Li ordering, suggesting the presence of kinetic limitations and Li disorder, which might vary with the

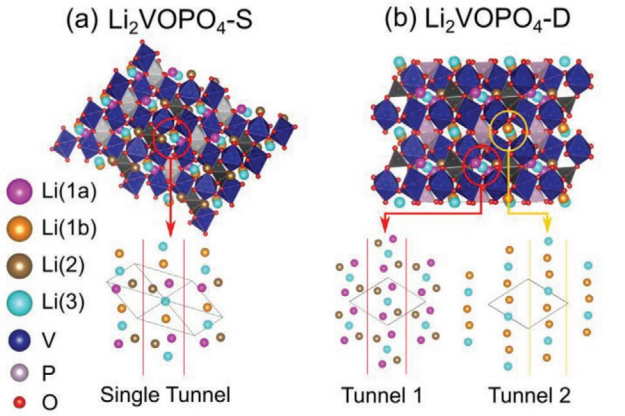

Figure 3. Two experimentally proposed Li orderings in ε-Li_2VOPO_4, which contain a) one (S) and b) two (D) distinct types of tunnels along the [110] direction, respectively, with the corresponding Li orderings shown beneath each structure.

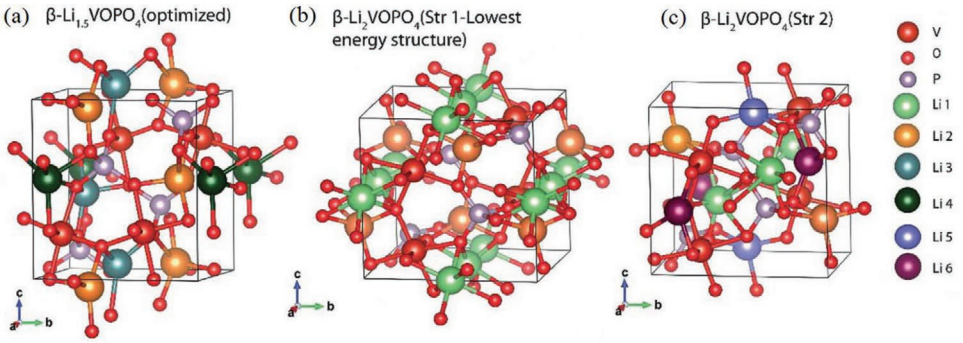

Figure 4. Crystal structure of a) β-$Li_{1.5}VOPO_4$ after optimization, b) β-Li_2VOPO_4 (Str 1) (lowest energy structure), and c) β-Li_2VOPO_4 (Structure 2, the most consistent with NMR data). Reproduced with permission.[25] Copyright 2020, The Royal Society of Chemistry.

sample synthesis method. The best insight into β-Li_2VOPO_4 structure was obtained from electrochemically lithiated nanocrystalline β-$VOPO_4$ synthesized from a H_2VOPO_4 precursor. The ^{7}Li NMR spectrum of this sample, in contrast to that of β-Li_2VOPO_4 sample obtained from β-$LiVOPO_4$, exhibits more intense and sharper peaks at 306 and 258 ppm, and much better resolved peaks at –18 and –44 ppm, which are assigned to Li ions in the environments more coordinated with O (i.e., Li1 and Li6). Similar to the sample obtained from β-$LiVOPO_4$, this spectrum also exhibits a sharp resonance at 60 ppm, a feature arising from the β-$Li_{1.5}VOPO_4$ phase. By comparison with the ^{7}Li NMR shifts obtained from DFT calculated structures and from the ^{7}Li correlation experiments, it is shown that the β-Li_2VOPO_4 NMR spectrum is more consistent with the calculated structure 2 in Figure 4, which has a slightly higher energy than the lowest energy structure for β-Li_2VOPO_4. Thus, β-Li_2VOPO_4 exhibits complex Li ordering, which depends on sample preparation route. It is consistent with previous studies by Harrison et al.,[18a] and our observations on Li ordering in ε-Li_2VOPO_4.

4. Reaction Mechanism

As was just shown, vanadium phosphates can intercalate up to 2 Li^+ ions per V, resulting in the transition of $VOPO_4 \leftrightarrow LiVOPO_4 \leftrightarrow Li_2VOPO_4$. Due to the differences in crystal structure, the voltage profiles of each polymorph are also expected to be different. Lin et al. showed using first principles calculations that the insertion of the first Li^+ results in voltages with the trend of $\beta > \varepsilon > \alpha_I$, which is in agreement with experimental profiles.[11,17] They also calculated that the insertion of the 2nd Li^+ into α_I-$LiVOPO_4$ will result in a single voltage plateau, which is in agreement with experimental profiles.[17] They predicted that the insertion of the 2nd Li^+ into β-$LiVOPO_4$ would result in two plateaus, with an intermediate phase of β-$Li_{1.5}VOPO_4$. Although the voltage profile overall fits experimental data,[17] the β-$Li_{1.5}VOPO_4$ could not be detected using XRD due to its similar structure to β-Li_2VOPO_4. As was discussed earlier, Britto et al. showed that this β-$Li_{1.5}VOPO_4$ can be observed when using solid-state NMR.[25] Finally, insertion of the 2nd Li^+ into ε-$LiVOPO_4$ was calculated to result in three voltage plateaus, with the intermediate phases of ε-$Li_{1.5}VOPO_4$ and ε-$Li_{1.75}VOPO_4$, both of which were observed experimentally.[10a,17] A comparison of the calculated and experimental voltage profiles is shown in **Figure 5**.

Although all polymorphs have poor ionic and electronic conductivities, historically, α_I- and β-$LiVOPO_4$ were considered the superior polymorphs in terms of electrochemical performance.[11,19,26] This was due mainly to ε-$LiVOPO_4$ being labeled as electrochemically inactive. Lin et al. showed that the diffusion barriers in β-$LiVOPO_4$ are lower than those of ε-$LiVOPO_4$.[11] Additionally, Hidalgo et al. predicted that β-$LiVOPO_4$ has more electrochemically active surfaces than ε-$LiVOPO_4$. They also used TEM to show that these facets naturally form during the formation of $LiVOPO_4$.[17] These explain Azmi et al.'s observations that pristine β-$LiVOPO_4$ has appreciable electrochemical performance, while pristine ε-$LiVOPO_4$ has almost no capacity.[26a]

First insights into the reaction mechanism of ε-$LiVOPO_4$ were given by Bianchini et al. and Lin et al. However, high-energy ball-milled materials were used in these studies limiting the quality of the diffraction data.[10a,19] We have further investigated the reaction mechanism of more crystalline ε-$VOPO_4$ using a combination of in situ powder diffraction and pair-distribution function analysis.[22] Powder diffraction data recorded during first lithiation and delithiation of monoclinic (Cc) ε-$VOPO_4$ (a = 7.2788(5), b = 6.8971(1), c = 7.2660(6), α = 90, β = 115.39(5), γ = 90) cycled within 1.6–4.5 V voltage window (**Figure 6**; Experimental Details in the Supporting Information), shows that structural transitions observed during cycling are symmetrical and largely reversible. The peak positions and trends observed here are consistent with ones observed during high voltage and low voltage cycling of ε-$LiVOPO_4$[10a,19] indicating that the reaction mechanisms for these compounds are independent of starting material. During the first electrochemical plateau at 4.0 V, for Li $0 \le x \le 1$, the reaction proceeds through a two-phase process with no observed intermediates. The resulting phase, ε-$LiVOPO_4$, is of triclinic space group $\overline{P}1$ with following lattice parameters: a = 6.7972(6), b = 7.2185(5), c = 7.8913(5), α = 90.084(4), β = 91.189(6), γ = 117.14(1). Subsequently, this newly formed phase, in the low voltage region, ($1 \le x \le 2$) intercalates a second Li ion through two stable intermediate phases, at x = 1.5 and 1.75, consistent with the three electrochemical plateaus observed. Both $Li_{1.5}VOPO_4$ (a = 7.067(4), b = 7.800(9), c = 7.130(0), α = 89.679(3), β = 116.18(7), γ = 89.848(9)) and $Li_{1.75}VOPO_4$ (a = 7.516(5), b = 10.545(5), c = 10.519(7), α = 84.396(4), β = 69.791(6), γ = 110.77(9))

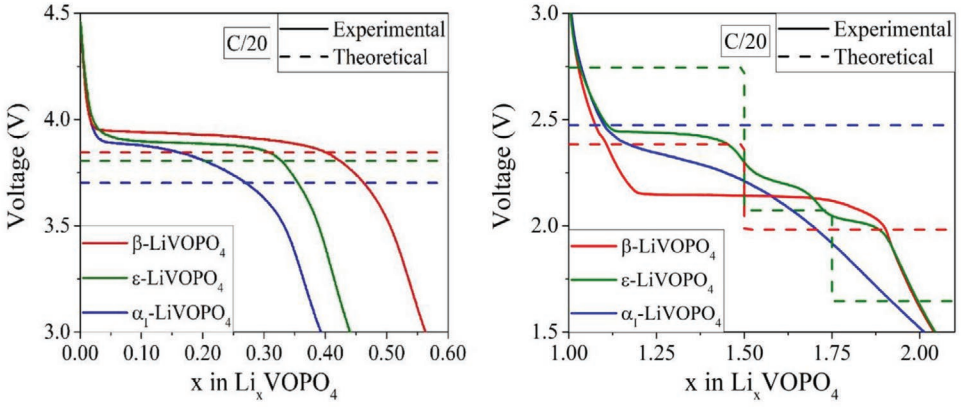

Figure 5. Comparison of calculated (dashed) and experimental (solid) voltage profiles in the high- (left) and low-voltage (right) regions. Reproduced with permission.[17] Copyright 2019, The Royal Society of Chemistry.

structures have $\overline{P}1$ symmetry, albeit the best fit for $Li_{1.75}VOPO_4$ data is achieved with a model of a supercell twice the size that of the Li_2VOPO_4 (a = 7.205(6), b = 7.123(7), c = 7.800(8), $\alpha = 90.003(3)$, $\beta = 89.727(3)$, $\gamma = 116.453(0)$).

Upon charge the process is reversed with all intermediates visibly forming in predictable sequence. Final charge product closely resembles the original monoclinic (Cc) ε-$VOPO_4$ material with the lattice parameters of a = 7.2894(2), b = 6.9086(8), c = 7.2663(0), $\alpha = 90$, $\beta = 115.42(1)$, $\gamma = 90$ and slightly reduced coherence.

Even though based on the X-ray powder diffraction data, phases involved in ε-$LiVOPO_4$ and ε-$VOPO_4$ electrochemical cycling appear to be the same, the electrochemical performance differences reflected in efficiency of cycling and hysteresis are evident. Pair distribution function analysis of the total scattering data collected during cycling indicates subtle difference in local V environment behavior for these two compounds cycled in a low voltage window. These changes in the local structure can be quantified by fitting Gaussian functions to features in the PDF, where the change in peak positions reflect changes in the average bond lengths, while the changes in peak areas correspond to changes in the average coordination number. Based on the Heyd–Scuseria–Ernzerhof (HSE) calculations Li_xVOPO_4 have symmetrically distinct VO_6 local environments that evolve during cycling. For instance, V^{+5} within ε-$VOPO_4$ has an asymmetric coordination environment, with one short V=O bond (1.57 Å) one long V—O (2.62 Å) and four intermediate V—O (Å) bonds; V^{+4} within ε-LiVOPO4 also has an asymmetric coordination environment, with one short V=O bond (1.62 Å) and five intermediate V—O bonds (1.92 Å) and finally, V^{+3} within Li_2VOPO_4 has symmetric coordination with six bonds averaging (2.035 Å). Careful PDF analyses can easily resolve the difference between short, long and intermediate bond lengths, however it should be noted that the short V=O bond at ≈1.6 Å overlaps with the contribution from the P—O correlations within the PO_4^{3-} anion. Since the rigid geometry of the PO_4 polyatomic anion is not expected to change significantly during cycling, all changes associated with the 1.6 Å feature can be entirely attributed to changes in the V=O bond.

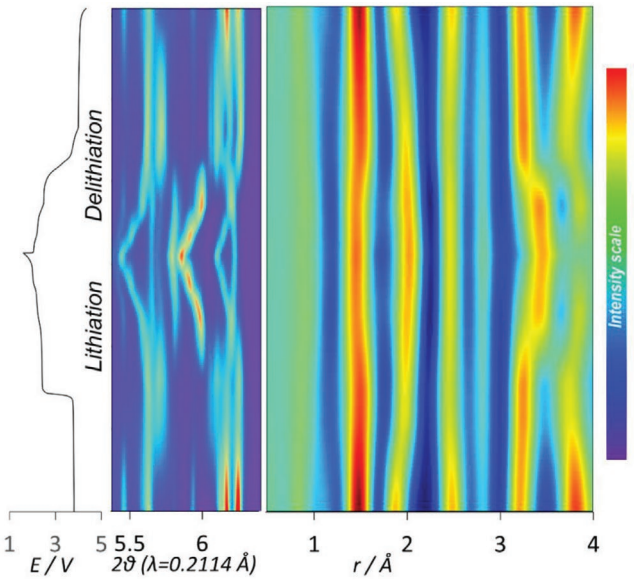

Figure 6. Contour map of selected intensities of powder diffraction data (middle) and PDFs (right) obtained by Fourier transforming the total scattering X-ray data collected during the initial discharge–charge cycle for $VOPO_4$/C electrode, cycled at C/15 rate within 1.6–4.5 V window (left). The colors reflect relative peak intensities.

Previously, our PDF analysis of the local structure of ε-$LiVOPO_4$ during cycling suggested, that during charge some of the bonds might have elongated beyond the HSE predicted model, suggesting irreversible decrease in V coordination number to below 6 (**Figure 7**). This was manifested by an overall loss in the intensity of the PDF feature corresponding to intermediate bond-lengths, accompanied by an unexpected increase in peak intensities around 2.6 Å. Based on the DFT-suggested relaxations of $HVOPO_4$ and H_2VOPO_4, we speculated that observed intensities >2.4 Å could be explained by H incorporation as a result of hydrate formation due to unintended catalytic electrolyte decomposition. It is also supported by our study of reactions between $LiVOPO_4$ and electrolyte resulting in formation of $HVOPO_4$ and H_2VOPO_4.[5]

The operando PDF data, collected during ε-$VOPO_4$ lithiation and delithiation over 2 Li range shows evolution of the local atomic structure during cycling (Figure 6). Here PDF data does not suggest major irreversible transformations in the vanadium

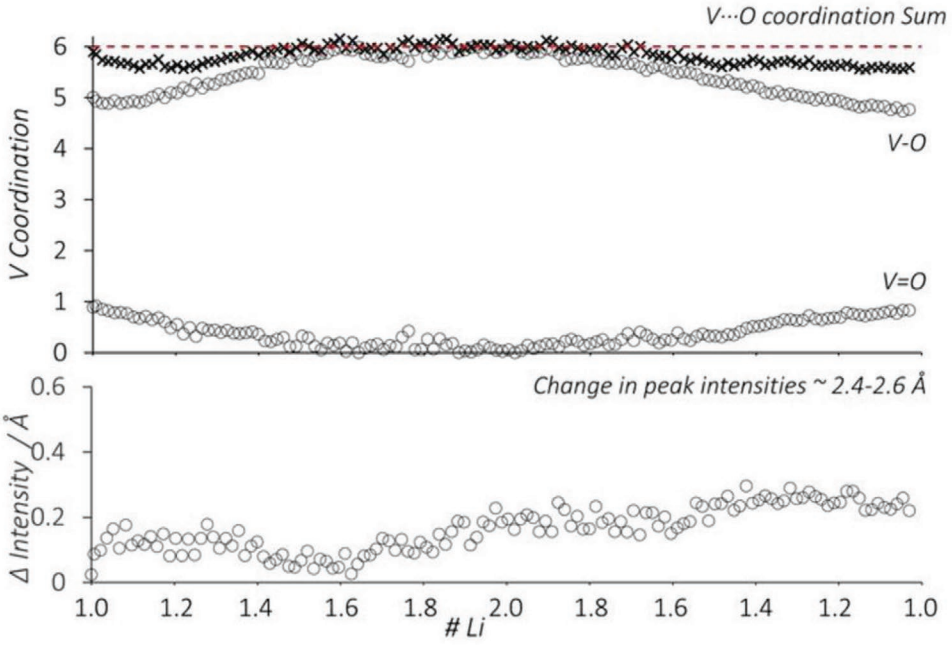

Figure 7. Average coordination number of V based on the intensity of selected peaks within the PDFs. Reproduced with permission.[19] Copyright 2016, The American Chemical Society.

environment. Both the areas (**Figure 8**) and positions (**Figure 9**) of the peaks at 1.6° and 2.0° and 2.6 Å linked to the V—O bonding, quantified by fitting Gaussian peak profiles, show that bond lengths and vanadium coordination number are in good agreement with the DFT-relaxed VO_6 environments for all phases involved in the $VOPO_4$ reaction. This might suggest that controlling the particle size and morphology through synthesis is a better strategy to reduce side reactions in this system. For the best electrochemical performance, the $LiVOPO_4$ sample had to be heavily ball-milled with carbon and in that process the coherence of the sample was reduced to ≈6 nm. This could promote higher catalytic activity toward electrolyte decomposition. In ε-$VOPO_4$ the particle size of 100–200 nm may help to avoid or at least decrease efficiency of this catalytic reaction.

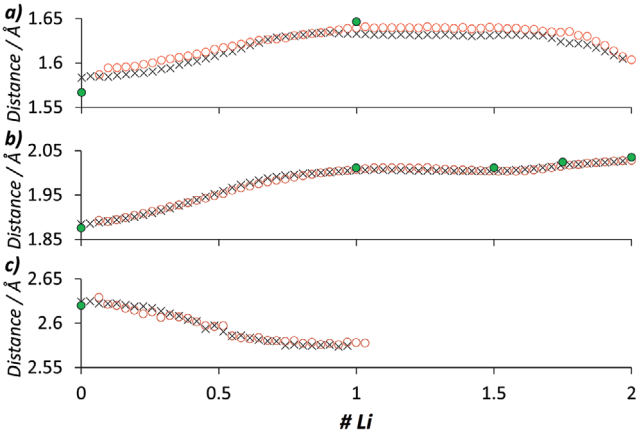

Figure 8. Evolution of peak positions corresponding to the V—O bonds changes during ε-$VOPO_4$, Experimental data, black crosses discharge, open red markers charge; HSE calculated distances, green closed markers.

5. Synthesis and Its Impact on the Electrochemical Performance of (Li)$VOPO_4$

As follows from the existence of several energetically close polymorphs, synthesis plays a key role in obtaining pure phase $LiVOPO_4$ materials. Different synthesis methods yield various levels of crystallinity, particle sizes, and defects, all of which radically change the material's electrochemical properties. Additionally, each method varies in terms of cost and complexity, both significant factors in the manufacturing of these materials. A prime example of this is $LiFePO_4$. Despite its intrinsically poor conductivity, it has become one of the most successful Li-ion battery materials. This was achieved through a combination of synthesizing nanosized particles[27] as well as the formation of a conductive carbon coating[28] upon synthesis or postheating. The reduction of particle size mainly improves the conductivity by shortening the diffusion pathway of Li-ions, allowing them to more easily participate in redox reactions. In 1D diffusion materials, it has the added benefit of reducing the chance of a channel being blocked by defects.[29] The conductive coating improves the electronic conductivity of the cathode as a whole, allowing redox reactions to occur more easily, while also protecting the solid-electrolyte interface (SEI) from getting damaged.

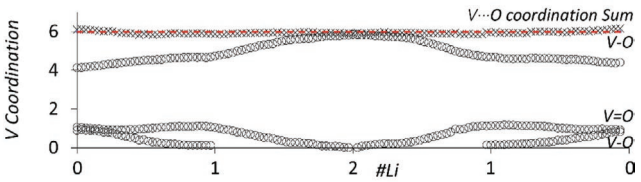

Figure 9. Average coordination number of V within ε-$VOPO_4$ during cycling, based on the peak areas of selected peaks within PDF.

The similarities between $LiFePO_4$ and $LiVOPO_4$ in terms of poor intrinsic conductivities and 1D diffusion in some polymorphs,[8b,19] suggest that similar strategies of nanosizing and carbon coating should be useful. However, the $LiVOPO_4$ synthesis is complicated by its polymorphism, and the fact that it is reduced upon high-temperature carbothermal treatment[30] widely used in $LiFePO_4$ synthesis to simultaneously carbon-coat and control particle size. This further emphasizes the challenges that the successful synthesis approaches should address.

There are several methods for synthesizing $LiVOPO_4$, the most commonly used ones being the solvothermal (ST),[7b,18c,31] sol–gel (SG),[18b,26,32] solid-state (SS)[10a,19,20,30,33] methods, or by using a $(Li)VOPO_4{\cdot}2H_2O$ precursor.[7a,17,34] We placed general information on advantages of each of these approaches in the Supporting Information, and will focus here on the application of these methods to $LiVOPO_4$ synthesis.

5.1. Solvothermal Method

The main advantage of the solvothermal method and its microwave-assisted variation (MWST) is the low synthesis temperature, which makes the method cost-effective, and allows access to metastable phases. Also, control of solvent and synthesis time provides a route to small particle size. The work of Harrison et al. comprises a thorough study of the MWST method in synthesizing $LiVOPO_4$ focusing on the investigation of the various parameters affecting the formation of each polymorph of $LiVOPO_4$ and their electrochemical performances in the high-voltage window.[31a] It is shown that, excess of Li and P help to drive the reaction toward the formation of $LiVOPO_4$. For example, having stoichiometric amounts of Li and V results in $HVOPO_4$ being the majority product, while having a large excess of Li results in the formation of Li_3PO_4 as the major product. The ideal ratios of Li, V, and P vary depending on the solvents used and the desired polymorph to be synthesized. The α_1 polymorph preferentially forms over the other polymorphs in water-rich solvents. This is possibly due to the similarity of α_1-$LiVOPO_4$ to $LiVOPO_4{\cdot}2H_2O$. On the other hand, the ε polymorph forms instead of the α_1 or β polymorphs if the temperature or pressure is increased. A similar observation was made by Chung et al., where the solvothermal synthesis at 160 °C resulted in $LiVOPO_4{\cdot}2H_2O$ while the product at 180 °C was ε-$LiVOPO_4$.[31d] Lii et al. have shown that β-$LiVOPO_4$ can be synthesized using the traditional solvothermal method at 230 °C.[7b] This means that higher temperatures are not the sole factor in determining whether the β or ε polymorph forms in the ST method. It is possible that the temperatures and pressures used in the study by Harrison et al. are close to the phase boundary between $\beta \leftrightarrow \varepsilon$, which would explain the big changes upon changing the temperature and pressure. However no such phase diagrams between β- and ε-$LiVOPO_4$ have been calculated yet.

The ST method, especially the MWST method, is also the method which generally results in small particle sizes, ranging from hundreds of nanometers to several micrometers. Harrison et al. varied surfactants and solvents (i.e., adding glycols) as well as synthesis time in order to reduce the particle size of the synthesized $LiVOPO_4$, with the goal of improving the electrochemical performance. Both approaches were successful, with the simplest and most significant improvement achieved by reducing the hold time from 50 to 10 min. This improved the capacity from 72 to 115 mAh g^{-1} over the voltage range of 3.0–4.0 V (C/20). However, the samples with smaller particle sizes experienced the greatest capacity fade, with all the samples eventually attaining very similar capacities after 20 cycles. This is probably due to an increase in the amount of side reactions which occur at the surface. Chung et al. and Kaplan et al. showed that the second Li can be cycled in hydrothermal and MWST ε-$LiVOPO_4$, respectively, achieving a capacity of more than 300 mAh g^{-1} over the voltage range of 1.5–4.5 V.[31d,35] It must be noted, however, that both methods resulted in large particles, thus requiring particle size reduction via high-energy ball-milling.

Chung et al. pointed out that one side effect of the ST method using water as the solvent is that protons intercalate into the $LiVOPO_4$ structure.[31d] This is clearly seen in the summary of the unit cell volumes from various synthesis methods shown in **Figure 10**, where ST methods generally have larger unit cell volumes for all polymorphs among the different synthesis methods. Kaplan et al. show[35] that these protons seem to be beneficial to the initial electrochemical performance of $LiVOPO_4$, but also result in more significant capacity fading when compared to the $LiVOPO_4$ without protons.

5.2. Sol–Gel Method

In the SG method, reagents are dissolved in a solvent (sol) with a gelation agent. After drying off the solvent, a 3D network with numerous submicrometer pores (gel) forms, which upon further annealing often leads to final product with large surface area advantageous for electrochemical performance.[36] Zhou et al. have investigated the SG method for synthesizing $LiVOPO_4$, showing the various phases that form while heating the gel in air. Three distinct products form at different temperatures: a low-temperature ε-$LiVOPO_4 \rightarrow \beta$-$LiVOPO_4 \rightarrow \varepsilon$-$LiVOPO_4$. Interestingly, this is also observed when heating amorphous $LiVOPO_4$ in O_2 (Figure S1, Supporting Information). If this amorphous $LiVOPO_4$ is instead heated in Ar, the low-temperature ε-$LiVOPO_4$ also forms, but does not transform into β-$LiVOPO_4$. Instead, at ≈500 °C it forms highly crystalline ε-$LiVOPO_4$. These suggest that ε-$LiVOPO_4$ more easily forms than β-$LiVOPO_4$ when starting with an amorphous material. This low-temperature, low-crystalline ε-$LiVOPO_4$ would then increase in crystallinity at around 500–600 °C. However, if O_2 is present, then the $\varepsilon \rightarrow \beta$ transition accompanies this increase in crystallinity. The final $\beta \rightarrow \varepsilon$ transition at extremely high temperatures occurs due to the formation of O-defects discussed in Section 2.

Kuo et al.[32f] and Allen et al.[18b] have also shown that if the calcination is conducted in an inert or reducing atmosphere, the β polymorph does not form, with the main product being the ε polymorph instead. This fits with the prediction that ε-$LiVOPO_4$ forms in the presence of O-vacancies, which easily form in the reducing/inert atmosphere. Conversely, Allen et al. show that β-$LiVOPO_4$ can be formed in a reducing/inert atmosphere given extremely low flow rates. They argue that the lower

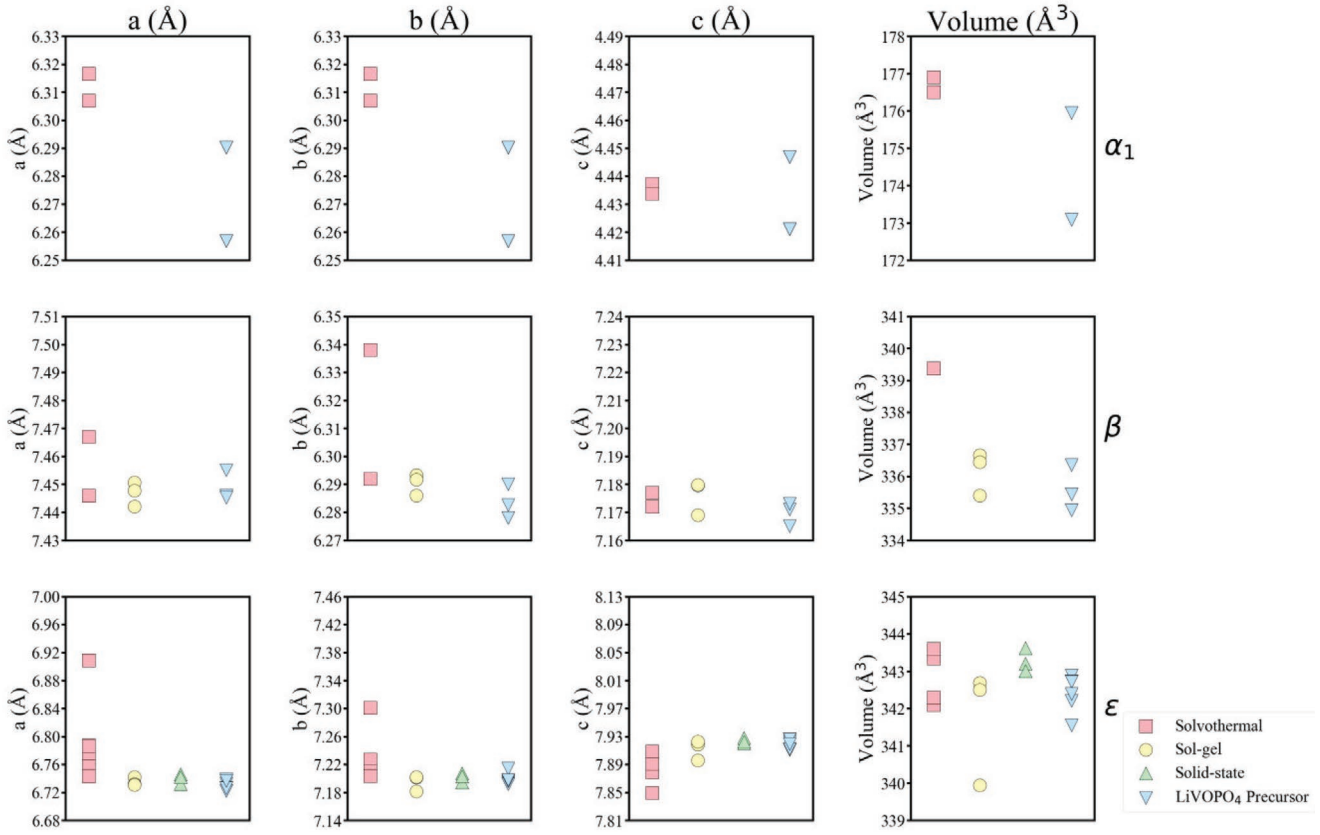

Figure 10. A comparison of the unit cell volumes of each $LiVOPO_4$ polymorph from various studies.[7a,b,17,18b,c,20,31a,d,32d,e,33a,34]

flow rates cause NH_3 (a reducing agent) to linger within the furnace longer, causing the gel to be reduced, which then results in β-$LiVOPO_4$. However, they do not show that β-$LiVOPO_4$ is O-poor, which is the opposite of what Hidalgo et al. observed.[17] Thus, we believe that it is also possible that the low flow rate simply caused air to remain within the furnace, which resulted in the formation of β-$LiVOPO_4$ instead of ε-$LiVOPO_4$. Overall, the SG method results in β-$LiVOPO_4$ when heated between 500 and 600 °C in air. On the other hand, it results in ε-$LiVOPO_4$ when heated between 500 and 700 °C in air or an inert atmosphere. This makes the method a good way to compare the β and ε polymorphs. Unfortunately, α_1-$LiVOPO_4$ cannot be synthesized using this method due to the high temperatures required.

Due to these high temperatures, the particle sizes from the SG method tend to be larger than those synthesized using the MWST method. At very high temperatures, the primary particles also begin to melt together. Thus, a high-energy ball-milling (HEBM) step may be needed for these materials to gain appreciable electrochemistry. The study by Azmi et al. is a good starting point to show this. They compared the electrochemical performance in the high-voltage window of a low-crystalline β-$LiVOPO_4$, high crystalline β-$LiVOPO_4$ and high crystalline ε-$LiVOPO_4$, all without HEBM.[26a] They show that the high-crystalline β-$LiVOPO_4$ has better electrochemical performance than the low-crystalline β-$LiVOPO_4$, improving the capacity from 75 to 95 mAh g^{-1} (C/50) within the voltage range of 3.0–4.5 V. This suggests that crystallinity plays an important factor in the electrochemical performance of $LiVOPO_4$. This is important because HEBM reduces the particle size while also reducing the crystallinity,[20,32d] and its implications will be discussed in Section 5.4. In a later publication, Azmi et al. also showed that HEBM can be used to further improve the electrochemical performance of β-$LiVOPO_4$, increasing the capacity to 120 mAh g^{-1} under the same conditions.[37] They show that this improvement was due to the reduction in particle sizes from 1 to 5 µm to submicrometer sizes.

The ε-$LiVOPO_4$ synthesized from their original study had a capacity of 10 mAh g^{-1} under the same conditions.[26b] This can then be compared to the study by Allen et al., where both the β and ε polymorphs were also synthesized using the SG method.[18b] They subjected the ε-$LiVOPO_4$ to HEBM before electrochemical testing, resulting in a decrease in the particle sizes from 2–5 to 1 µm. This improved the electrochemical performance by 100 mAh g^{-1}, achieving a capacity of 110 mAh g^{-1} within the voltage range of 3.0–4.5 V (C/50).

Zhou et al. compare the electrochemical performance of the low-temperature ε-$LiVOPO_4$, high-crystallinity β-$LiVOPO_4$, and high-crystallinity ε-$LiVOPO_4$ formed from their SG method over both high- and low-voltage windows.[32d] They utilized HEBM for all products, meaning the particle sizes were all the same prior to electrochemical testing. They show that the low-temperature ε-$LiVOPO_4$ has slightly higher capacity than the other products at 260 mAh^{-1} g within the voltage range of 1.5–4.5 V (C/10, C = 1 Li). They attribute this to the excess carbon within this sample which would theoretically improve the conductivity of the material. The β- and ε-$LiVOPO_4$ also attained high

capacities of 240 mAh g^{-1} under the same conditions. These studies all show that although the SG method can result in fairly small particles, these are often still too large for adequate electrochemical performance, especially with ε-$LiVOPO_4$.

One final interesting twist related to the SG method is the use of microwave sintering (MS) instead of traditional thermal conduction/convection/radiation heating of the gel.[38] As with the MWST method, the use of MS directly heats the gel and the reactants. This results in faster heating rates, more even distribution of heat, and faster reaction kinetics. These translate to lower energy costs, shorter heating times, and more uniform products, all of which are very attractive to manufacturing. This method has been shown to work with $LiFePO_4$, resulting in powders with smaller and more uniform particles.[39] As with the MWST method, a microwave absorber is needed, often a carbonaceous material. In the SG method, the gel serves this purpose. Wang et al. utilized this microwave sintering sol–gel method to synthesize β-$LiVOPO_4$.[32e] This resulted in highly crystalline products with particle sizes in the range of hundreds of nanometers, much smaller than any other SG method. The β-$LiVOPO_4$ synthesized using this method attained full 1 Li cycling, with capacities of 135–155 mAh g^{-1} within the range of 3.0–4.4 V (C/20). This further shows that good crystallinity and small particle sizes, regardless of the specific synthesis method, are critical to attaining good electrochemical performance.

5.3. Solid-State Method

The study by Shi et al. provides the mechanisms involved in the SS method for synthesizing $LiVOPO_4$.[20] Through in situ XRD with heating in Ar, they show that $LiVOPO_4$ does not form until ≈650 °C, with good crystallinity and purity not being achieved until 750–800 °C. This temperature is above the $\beta \rightarrow \varepsilon$ transition temperature, meaning the only phase possible using the SS method is ε-$LiVOPO_4$. The ε-$LiVOPO_4$ from this method synthesized had primary particles in the range of 1–2 µm, fused together into larger clumps with sizes > 10 µm. These large particle sizes are due to the high temperatures and long sintering times. Thus, HEBM will be needed in order to achieve any appreciable electrochemical performance. They show that ball-milled ε-$LiVOPO_4$ has smaller primary particles < 1 µm, which would help improve the electrochemistry. Unfortunately, the surfaces are also rough and the crystallinity becomes poorer with ball-milling, which would negatively affect the cycling stability. They show that too little ball-milling results in an overall lower capacity while too much ball-milling results in a good initial capacity but significant capacity fade. However, they show that almost 2 Li cycling was possible, with a capacity of 300 mAh g^{-1} at a slow rate (C/50, C = 1 Li). Overall, the SS method is the simplest of the 3 methods discussed, but also the most limiting.

The various synthesis conditions related to the formation of $LiVOPO_4$ are summarized in **Figure 11**; and Table S2 (Supporting Information). The reason that α_I-$LiVOPO_4$ has been shown to only form using the ST method or through the dehydration of $LiVOPO_4 \cdot 2H_2O$ is due to it being a metastable phase. Both β- and ε-$LiVOPO_4$ have similar thermodynamic stabilities, though ε-$LiVOPO_4$ is preferred when O-vacancies are present. Thus, ε-$LiVOPO_4$ can be synthesized at high temperatures using all the methods described above, where O-vacancies can be easily formed. β-$LiVOPO_4$ can also be synthesized using these methods, with the exception of the SS method, due to the high temperatures associated with SS.

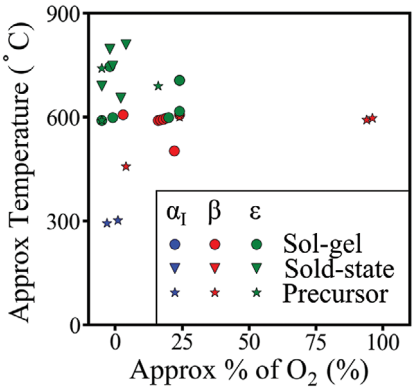

Figure 11. Synthesis conditions for various $LiVOPO_4$ phases.[7a,b,17,18b,c,20,31a,d,32d,e,33a,34]

5.4. Role of Disorder in Electrochemical Performance of ε-Li_xVOPO_4

When $LiFePO_4$ was first introduced, it faced the same problems of poor electrochemical performance due to poor ionic conductivity. The solution to this problem was nanosizing and the use of a conductive carbon additive. Shi et al. showed that utilizing these same methods, ε-$LiVOPO_4$ electrochemically comparable to other polymorphs can be made.[20] Specifically, in this work the HEBM method was optimized to reduce the particle sizes of ε-$LiVOPO_4$ from several microns to hundreds of nanometers. They also used various carbon additives, with the most promising being acetylene black or graphene nanoplatelets.

As discussed in the previous synthesis section, HEBM has proven to be an invaluable tool in improving the electrochemical performance of $LiVOPO_4$ by reducing the overall particle sizes. This is especially important for the β and ε polymorphs (in which Li undergoes 1D and pseudo-1D diffusion, respectively),[11,19] since smaller particle sizes would also reduce the chance for defects to block the diffusion pathways.[29] HEBM would be especially important for ε-$LiVOPO_4$ because it exposes more facets which could be electrochemically active.

Unfortunately, HEBM also induces strain and results in a significant loss in crystallinity.[20] Rana et al. showed that the $VOPO_4 \leftrightarrow LiVOPO_4$ reaction is plagued with side reactions, possibly due to the formation of a semireversible SEI.[12,40] This is shown in **Figure 12**, where the measured capacity (red squares) is much larger than the capacity due to V redox (red diamonds). They also mentioned that these side reactions are not observed in nanosized samples which did not undergo HEBM.[13] Thus, they attributed these side reactions and the sluggish $V^{4+} \leftrightarrow V^{5+}$ redox reaction to the disorder induced by HEBM.

In another study by Shi et al., it was shown that annealing the disordered ε-$LiVOPO_4$ after HEBM can be used to reduce the disorder and improve the electrochemical performance.[30] First, XRD shows that annealing causes the ε-$LiVOPO_4$ peaks to sharpen, which are indicative of improved crystallinity. ^{7}Li

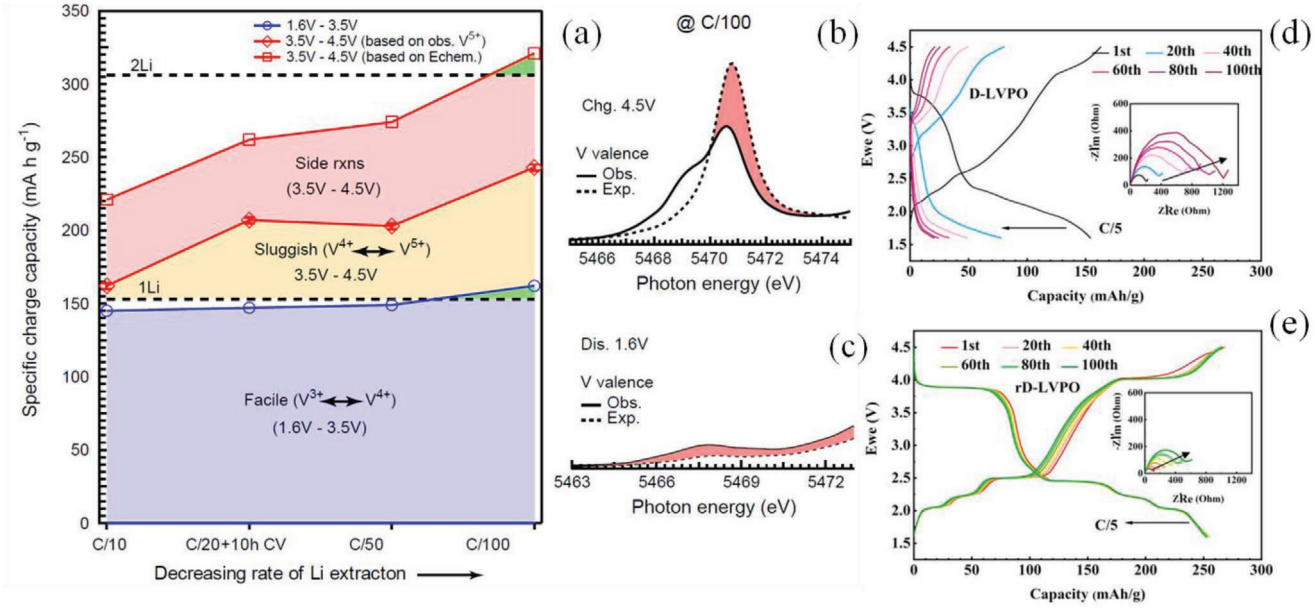

Figure 12. a) Comparison of capacity due to V redox and side reactions within the disordered ε-$LiVOPO_4$, with specific V pre-edge features showing sluggish b) $V^{4+} \rightarrow V^{5+}$, and c) $V^{4+} \rightarrow V^{3+}$ redox;[40] comparison of the electrochemical performance of the d) disordered and e) reduced-disordered ε-$LiVOPO_4$.[30] Plots (a–c) are reproduced with permission.[40] Copyright 2018, The Royal Society of Chemistry. Plots (d) and (e) are reproduced with permission.[30] Copyright 2019, Elsevier.

NMR also shows that HEBM causes an increase in the amount of Li residing in the 2nd Li site, which is associated with the disordered phase. Upon annealing, the NMR peaks associated with the disordered sites decreased, showing a decrease in the overall disorder. Similar observations were made using ^{31}P NMR. PDF also showed increased structural coherence and lower V thermal parameters after annealing, both of which are associated with a decrease in disorder. Overall, annealing has been shown to improve the crystallinity of ε-$LiVOPO_4$ while maintaining its purity.

Electrochemical tests also show that the reduced-disorder sample has superior electrochemical performance, only experiencing ≈4% capacity fade after 100 cycles. This is compared to the disordered sample, which lost ≈85% of its capacity by 100 cycles. Additionally, the reduced-disorder sample has higher capacity, improved rate capability, higher Li^+ diffusion, and lower charge transfer resistances.[30]

Overall, HEBM has proven to be an invaluable tool in improving the electrochemical performance of $LiVOPO_4$. However, it also induces a large amount of strain and disorder, which are detrimental to the electrochemical performance of $LiVOPO_4$. Thus, either the disorder must be removed via annealing or the as-synthesized $LiVOPO_4$ must already have nanoscale particles while maintaining high crystallinity.

5.5. Nanocrystalline ε-$VOPO_4$ as a Model Material Achieving 2Li Cycling

The above review of the synthesis and electrochemical performance of $LiVOPO_4$ clearly indicates that well-crystalline nanosized (Li)$VOPO_4$ is required to achieve stable 2Li cycling. Such material was synthesized by Siu et al.[13] using H_2VOPO_4 as a precursor and heating it in O_2 at 550 °C, ε-$VOPO_4$ nanocrystals with cuboid particles of 100–200 nm were obtained (**Figure 13**). This material when coated with graphene nanoplatelets during electrode preparation delivers full theoretical capacity at C-rate (C = 2Li) up to C/20 for up to 50 cycles. X-ray absorption data confirms the reversible vanadium oxidation change from 3+ to 5+ upon Li cycling, indicating that the electrochemical capacity originates from vanadium redox rather than side reactions. As previously discussed, the ^7Li and ^{31}P NMR also confirms lithiation to Li_2VOPO_4 upon discharge. The only drawback of this material is sluggish kinetics of the high-voltage process, which worsens overall rate performance.

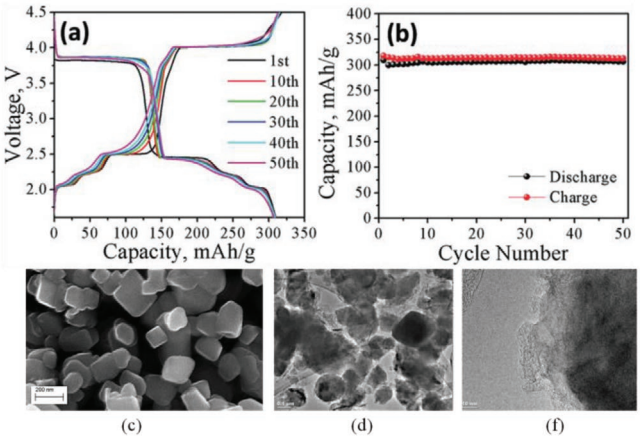

Figure 13. a) Galvanostatic charge–discharge curves of ε-$VOPO_4$ from 1.6 to 4.5 V and b) cycle performance at C/50, 1C = 2 Li; c) SEM image and c,d) TEM images of ε-$VOPO_4$ particles hand mixed with graphene nanoplatelets for slurry preparation. Reproduced with permission.[13] Copyright 2018, The Royal Society of Chemistry.

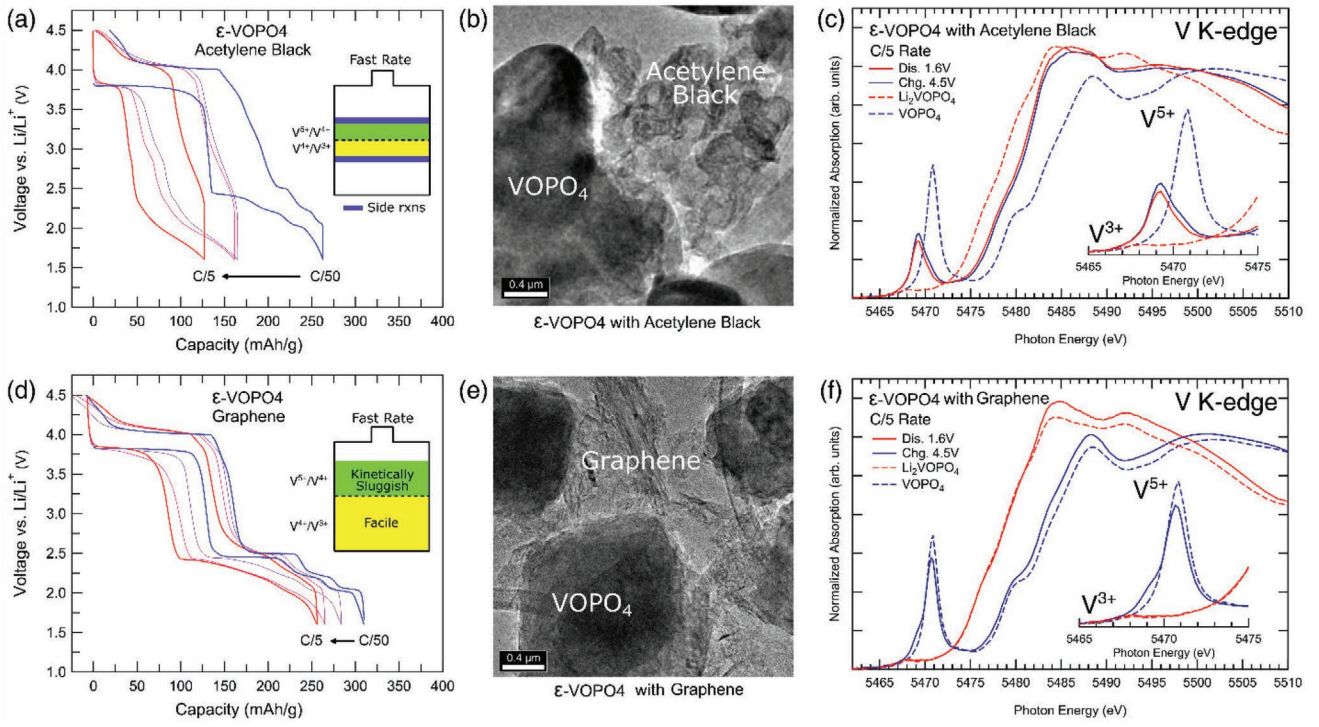

Figure 14. Electrochemistry of ε-$VOPO_4$ with Acetylene Black (Alfa-Aesar) a) and graphene nanoplatelets d) at different rates. TEM images showing particle to carbon contact for acetylene black b) and graphene e). Operando V K-edge XANES spectra with pre-edge inset depicting V valence for ε-$VOPO_4$ using acetylene black c) and graphene f) at high c-rate of C/5.

5.6. Role of Carbon Coating

ε-$VOPO_4$ with higher carbon content (70% Active, 20% Carbon, 10% PVDF) were used to decouple the role of carbon as it affects the electrochemistry of ε-$VOPO_4$ (see Experimental Details, Supporting Information). To minimize the effect of disorder induced nanosizing by way of ball-milling,[40] highly crystalline ε-$VOPO_4$ was used which can be synthetically nanosized[13] without the need to ball-mill. Due to the inherently poor conductivity of phosphate cathode systems, the addition of conductive carbon is required for proper electrochemistry. ε-$VOPO_4$ with acetylene black (Alfa-Aesar) carbon displays poor electrochemistry by not reaching theoretical capacity of 305 mAh g^{-1} (**Figure 14**a), even at a slow rate of C/50. The underperforming electrochemistry is largely attributed to the poor contact between the carbon and nanoparticle surfaces (Figure 14b). Operando V K-edge XAS spectra reflect the inactivity of ε-$VOPO_4$ with acetylene black at high rates of C/5 (Figure 14c). Due to capacity and V valence discrepancies, we suspect the catalytic behaviour of e-$VOPO_4$ to be activated when conductivity requirements are not met. Nanosized particle $VOPO_4$ in combination with highly conductive graphene nanoplatelets (xGnP), enables fully reversible theoretical capacity at C/50 (Figure 14d). The better performance stems from better carbon coverage (Figure 14e) effectively coating the ε-$VOPO_4$ nanoparticles. While the reversibility of ε-$VOPO_4$ with graphene decreases at higher rates, operando XAS measurements reveal V redox is active and proportional to the capacity at high rate of C/5 (Figure 14f). A point that should be made is that the better performance of graphene over acetylene black is not due to unique properties of graphene, but rather the surface area differences between the two carbons. The choice of carbon additive should be partial toward high conductivity and high surface area. While better conductive carbon can help acitvate more true V redox, the true catalytic behavior of vandyl phosphates is largely unknown and warrants further study.

6. Role of Substitution

With an electronic bandgap of ≥2.1 eV, all (Li)$VOPO_4$ polymorphs are considered to be either wide bandgap semiconductors or insulators.[19,26b] This wide bandgap is the cause of poor conductivity that inhibits electronic and Li-ion transport. Poor kinetics compounded with large particle sizes are key drawbacks restricting (Li)$VOPO_4$ from being suitable for most commercial applications. As previously discussed, HEBM has been introduced to decrease particle size as well as coat the material with a conductive carbon layer; however, it introduces a large amount of structural distortion that imposes kinetic limitations upon the $LiVOPO_4$ system.[40] A nanosized $VOPO_4$ material was obtained by Siu et al. to avoid the HEBM step; however, there is still a reduced capacity retention at fast rates.[13] Improvements to the high voltage kinetics, hysteresis, and capacity retention for (Li)$VOPO_4$ are still needed.

Transition metal substitution is a method that can be used to address these issues by altering the intrinsic properties of the material. This approach can be divided into two categories:

isovalent and aliovalent cationic substitution. The concept of the latter has been perceived with more skepticism. Complications in charge compensation can cause oxygen or lithium defects, or even change the oxidation state of the original transition metal. Computational studies of substituted $LiFePO_4$ (LFP) report unfavorable conditions for substitution citing higher solution energies for aliovalent cationic substitution than for isovalent substitution.[41] While some experimental results agreed with computational findings,[41b,42] other studies show successful isovalent and aliovalent substitution.[43]

The key to successful substitution, as both Omenya et al. and Harrison et al. point out, is reaction temperature. As reaction temperature increases, substituent solubility in the LFP system decreases. It is also seen that impurity phases increase with increasing temperature both demonstrating the need for lower reaction temperatures.[43b-e] A low-temperature synthesis method, microwave-assisted solvothermal synthesis, was used to ensure maximum substitution and found that up to 20% vanadium substitution into LFP was possible.[43e]

Similar to LFP, substitution into the $LiVOPO_4$ (LVP) system has mixed results depending on the synthesis method and temperature. A few groups claim to have substituted various transition metals into LVP using a high-temperature solid-state synthesis method. While they do mention electrochemical properties such as cycle stability[44] and conductivity[45] improvement, they provide little to no data to prove transition metal substitution occurred and was the key to these improved properties.

Lower temperature synthesis methods such as reflux,[46] sol–gel,[47] hydrothermal,[48] and microwave[35] were used for transition metal substitution into (Li)$VOPO_4$. Reflux methods were used to synthesize substituted vanadyl phosphate dihydrates, $VO(PO_4)\cdot 2H_2O$ (VOP), as well as two different substituted $VOPO_4$ polymorphs (α_{II}, δ) for catalytic purposes which are beyond the scope of this review. Substitution using up to 25% Mn,[46b] Fe,[46c–g] Ga,[46f] Al,[46f,g] Cr,[46f,g] and W and Nb[46h] were used. Wen et al. showed that up to 5% of Mo can be substituted into $VOPO_4$, using a hydrothermal method followed by annealing at 550 °C. It was shown that Mo is in the 6+ state in this compound compensated by equal amount of V^{4+}. Mo substitution was shown to enhance Li diffusion kinetics, leading to higher electrochemical capacity and better cycling stability.[48a]

We have extended this effort to investigate the possibility of substituting other transition metals similar to V in terms of ionic size, coordination, or oxidation states, using low-temperature hydrothermal and microwave-assisted hydrothermal methods. According to Vegard's law, as substitution occurs, we expect to see lattice parameter changes that correspond to an enlargement or shrinkage of the lattice depending on which substituent is being used.[49] Table S3 (Supporting Information) shows the ionic radii[50] of the substituents we used in their charge state detected by XAS. XRD analysis of these (Li)$VOPO_4$ materials show mostly pure (Li)$VOPO_4$ either in the epsilon phase, beta phase, or a mixture of both (Figure S2 and Table S4, Supporting Information). The hydrothermally synthesized materials indicate an $HLiVOPO_4$ impurity phase is present. It is more apparent in the Cr-substituted samples, however, HRXRD indicates the impurity is present in the Nb-substituted samples as well.[48c] For all syntheses, the substituted materials tend to prefer one phase over another, but with synthesis manipulation and post-annealing, a pure phase can be achieved.[48b]

As mentioned previously, different methods produce different lattice parameters for pristine (Li)$VOPO_4$ depending on how many defects were introduced into the structure during synthesis. According to TGA data, the synthesis methods using water as a solvent without a post annealing are more likely to have a greater number of protons in the structure, making the volume larger than the theoretical values.[31d] This holds for the substituted materials as well, which is why, in general, the hydrothermal (HyT) and microwave (MW) synthesized materials have larger volumes than not only the calculated pristine $LiVOPO_4$ but also the hydrothermal samples with postheating (HyTA) for both the pristine and substituted materials.

The lattice parameters, plotted against the experimentally determined substituent content detected by inductively coupled plasma (ICP) analysis (Table S4, Supporting Information) are presented in **Figure 15**. For ε-$VOPO_4$, increasing the amount of substituent increases the *b* lattice parameter while the *a* and *c* stay the same. The lithiated phase shows an increase in the *a*, *b*, and volume parameters, but a decrease in the *c* direction. For β-$LiVOPO_4$, there is an increase in all lattice parameters as the substituent content increases. Overall, there was an increase in volume for each of the substituents in all synthesis methods indicating a change in the (Li)$VOPO_4$ lattice. Based on the lattice parameters change, the substituents that have most likely substituted into the structure are Cr, Nb, Ti, and Mo, while W, Zr, and Mn are less likely to substitute.[48]

Lattice parameter changes are affected by the synthesis method, as seen in Figure 15. For the epsilon $LiVOPO_4$ phase, similar trends are seen to different extents. The two low-temperature methods—MW and HyT—show a larger increase in the *a* and *b* directions. While the HyTA synthesis products also show an increase in the *a* and *b* directions, but compared to the MW and HyT methods, the change is very slight. In the *c* direction, the HyTA samples show no change, however, the MW and HyT samples show a decrease as the substituent content increases. For the β-$LiVOPO_4$ phase, the two low-temperature methods show an increase in all the lattice parameters as the substituent content increases, while the HyTA method shows no change in the *c* direction and only minimal change in the *b* direction. The differences in these unit cell parameters could come from the presence of protons in the low-temperature methods.

XAS data were used to determine oxidation states of V and substituents and to derive the charge compensation mechanism in combination with ICP data. XAS data show Nb in the 5+ oxidation state with the majority of the vanadium in the V^{4+} for $LiVOPO_4$ and V^{5+} for $VOPO_4$.[35],[48] In order to charge compensate in the LVP system, lithium deficiencies were seen as the amount of niobium increases. Cr^{3+} also caused lithium and vanadium deficiencies, however, the number of protons increases to compensate for the loss of charge.[48c] Both Mo and W are in the highest oxidation state of 6+ which brings them to a similar ionic radius as V^{4+} in $LiVOPO_4$. Significant charge compensation must occur to compensate the higher charge of the substituents, and therefore the presence of V^{3+} is expected to be high as no lithium deficiencies were seen in ICP data

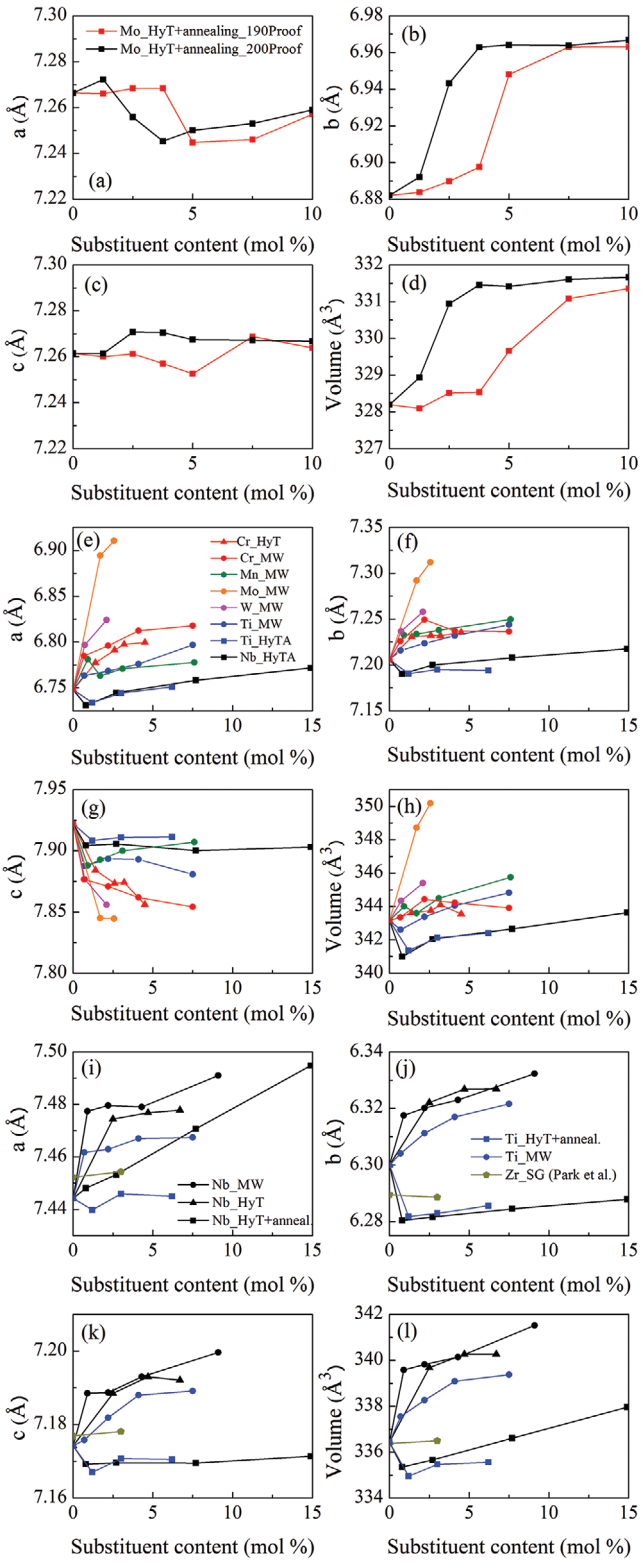

Figure 15. Lattice parameters and unit cell volumes of substituted a–d) ε-$VOPO_4$, e–h) ε-$LiVOPO_4$, and i–l) β-$LiVOPO_4$ synthesized via sol–gel (SG), microwave (MW), and hydrothermal (HyT) methods followed by annealing (HyTA).

(Table S4, Supporting Information). This is seen more clearly with the Mo-substituted samples, as more Mo is present overall in the material than W.[48a,c,d] Mn, however, is in the lowest oxidation state also having the largest ionic radius. It might be more difficult for the manganese to substitute into the structure because of the significant difference in size, however, the increase in volume from the protons in the microwave sample, may allow for the manganese to be inserted in the structure more easily. XAS shows no indication of V^{5+} present in the MW samples and there is also no change in lithium content suggesting Mn is not likely to substitute into the LVP structure.[35] The presence of V^{3+} and the larger substituent will both cause changes in the unit cell volume seen for all aliovalent cations. The increasing presence of protons might account for the changes seen in the Mn-substituted material. Overall, based off lattice parameter changes combined with XAS and ICP results there is strong evidence that Nb, Mo, W, and Cr do get incorporated into the $LiVOPO_4$ structure as aliovalent substituents.

XAS data indicate both Ti and Zr are isovalent to V^{4+} which means no charge compensation is necessary when these cations are substituted into the LVP structure. Calculations indicate the lattice parameters for the beta phase will not change significantly as substitution occurs, however there will be visible change in the epsilon phase.[48b] This is generally consistent with experimental data (Figure 15). It is important to remember here that the MW sample listed in Figure 14 is roughly 50% β-LVP and 50% ε-LVP. It is consistent with $LiTiOPO_4$ existing in polymorphs isostructural to both ε- and β-LVP.[51] The HyTA sample has the majority of the material in one phase or the other. They both show similar trends between the phases, making it difficult to determine if the Ti is substituted into one phase over the other in the MW material. Due to the slight increase in lattice parameters combined with ICP detection of the element, it is expected that the Ti does get incorporated into the LVP structure.

Due to the larger size of Zr^{4+}, it is expected there will be a large change seen in the unit cell volume as Zr gets substituted in. However, the experiments show virtually no change in lattice parameter, even after a 3% substitution reported by Park et al. While XPS data show Zn is present on the surface and ICP and EDS data additionally confirm the presence of Zr, these techniques cannot confirm that it has been successfully substituted into the crystal lattice.[47a] Kaplan et al. report Zr does not substitute into their MW material as the little Zr detected by ICP does not affect the lattice parameters.[35] While Zr is present in both samples, it cannot be concluded that it substituted into the crystal structure. In both materials, however, improvements were seen compared to the pristine material suggesting that a mechanism other than substitution, i.e., surface coating, may lead to better cycle life.

The best electrochemical performances out of the substituted (Li)$VOPO_4$ materials are summarized in **Figure 16**. It can be seen that substitution overall has improved cycle stability in comparison to the pristine counterparts. As mentioned previously, the carbon additive used during electrode preparation plays a factor in the electrochemical performance of (Li)$VOPO_4$. It is important to note here that different carbon additives and cycling rates were used for various studies. The MW samples

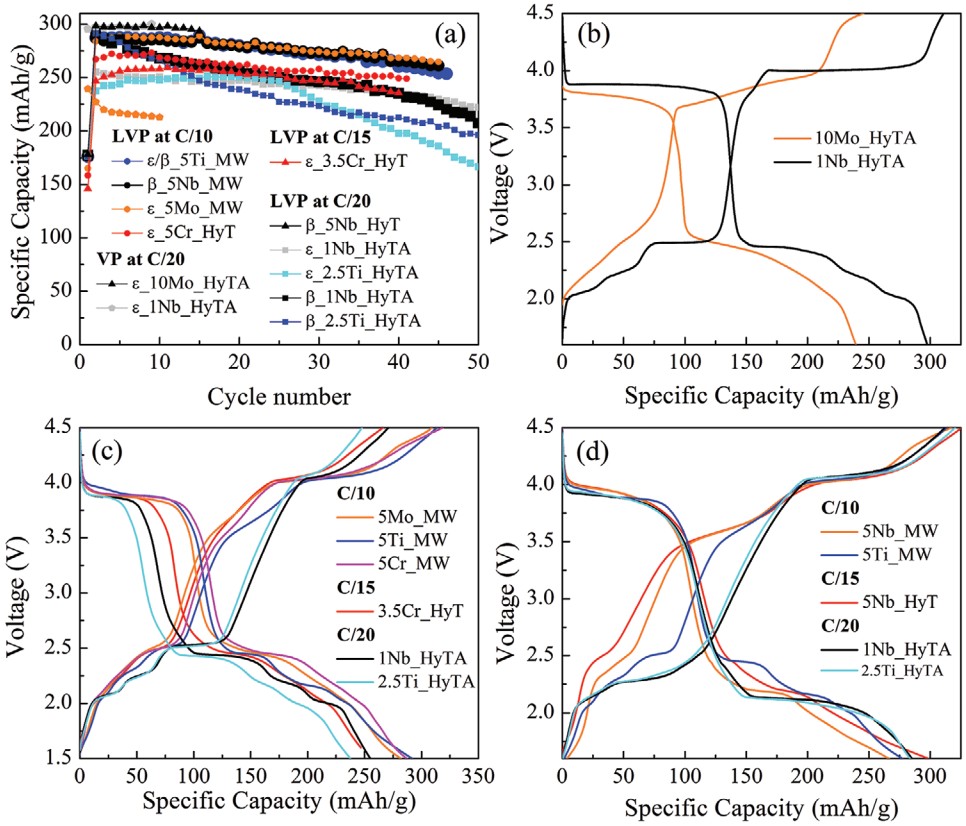

Figure 16. a) Cycling stability of all substituted samples and galvanostatic charge–discharge curves for b) ε-$VOPO_4$, c) ε-$LiVOPO_4$, and d) β-$LiVOPO_4$.

used graphene and were cycled at C/10 (C = 1 Li); the Cr HyT sample used acetylene black and was cycled at C/15 (C = 1 Li); the Mo HyTA sample used carbon black and was cycled at C/20 (C = 1 Li); the Nb HyT, and Ti and Nb HyTA samples used graphene and were cycled at C/20 (C = 1 Li).The materials with the same substituent perform differently depending on synthesis method. For the Ti-substituted materials, different phases are obtained in the different methods. The two 2.5% Ti_HyTA samples are pure phase beta or epsilon, while the Ti_MW sample is 50% each. The beta phase 2.5% Ti_HyTA experienced capacity fade for the initial 25 cycles and regained stable cycling thereafter. In contrast, the epsilon phase showed consistent capacity retention for the first few cycles but experienced a larger capacity fade after 25 cycles. The Ti_MW sample performed the best compared to the 2.5% Ti_HyTA samples, having the highest capacity and cycle stability. This may be due to the mixture of phases, or the presence of protons in the sample.

The Nb_HyTA sample shows the beta phase starts off with higher capacity than the epsilon phase, however, the epsilon phase shows steady capacity retention making it better for long-term cycling. The niobium samples without the postheating (MW, HyT) have much higher capacity, even at the faster rates. The slight increase in rate will contribute to the higher capacity seen for Nb_HyT, and is therefore comparable to the Nb_MW and Nb_HyT materials. Likewise, the Mo and Cr-substituted (Li)$VOPO_4$ samples prepared by different procedures also show varying results. For both substituents, the samples synthesized by MW present higher relative capacities, even at the slower rates. Although 10% Mo_HyTA shows the lowest capacity of all the samples, this material still demonstrates good capacity retention for 10 cycles. As for the Cr-substituted samples, while 5% Cr_MW initially has higher capacity, both HyT and MW samples show good stability for long term cycling. The Cr_HyT sample shows an improved coulombic efficiency of above 96% and a capacity retention of ≈95% after 40 cycles. A comparison between these low temperature methods, which both incorporate protons into the structure, shows that the addition of graphene likely contributes to the higher capacity of MW sample.

The substituted samples synthesized by low temperature methods (HyT and MW) contain an additional "bump" in the high voltage during the charging process which is also observed in the pristine samples. The annealed pristine MW electrode material does not contain this "bump" and therefore, it is tentatively attributed to the presence of protons.[35] The unresolvable voltage steps in the low-voltage area can also be attributed to the presence of protons which prevent Li ordering for these intermediate phases to form. Substitution increases these defects in the structure which further exaggerates this effect creating more of a solid-solution kind of voltage profile. Of note is that the HyTA samples also show the shortest high voltage plateau.

Similarly, in the beta phase, the HyTA samples again show profiles most similar to what is expected. In contrast to the epsilon phase, all samples have similar high-voltage plateaus, which can be correlated to better reaction stability and kinetics of the beta phase over the epsilon. The HyT and MW samples again have the extra step in the high voltage region and a

voltage step missing in the low voltage area. The exception is Ti_MW which shows a voltage profile more comparable to the epsilon phase. For the same substituents synthesized by low temperature methods (HyT and MW), Nb substitution causes the largest hysteresis.

Overall, the substitution in (Li)$VOPO_4$ is limited to several percent of either isovalent or aliovalent ions. The substituted samples synthesized by low-temperature hydrothermal methods tend to incorporate protons as a way of charge compensation for substitution or nonstoichiometry. Interestingly, these nonstoichiometric disordered samples show fairly good initial electrochemical performance. However, upon annealing this performance deteriorates, contrary to what happens to the disordered high-energy ball-milled samples upon annealing. It might be correlated to the nonstoichiometric nature of the hydrothermal samples, which might prevent ordering upon annealing.

7. $VOPO_4$ Materials for Na Cycling

Although Li-ion batteries are the most promising mode of energy storage for portable devices and electric vehicles, the rising cost and limited geographic distribution of Li drives the research into alternative chemistries. The best candidate is Na, the next element from the same family as Li.

Research on $NaVOPO_4$ is fairly limited. Lin et al. calculated the various thermodynamic properties of $NaVOPO_4$ and compared them with one another and with those of $LiVOPO_4$.[11] The calculations show that in the Na—V—P—O phase diagram, the energy of the $VOPO_4$ structure is closer to the convex energy hull than the $NaVOPO_4$ phase which in turn is significantly closer to the hull than the Na_2VOPO_4 phase.[11] This explains why there are no reports on the direct synthesis of Na_2VOPO_4. Additionally, very few studies directly synthesize $NaVOPO_4$,[52] with most other studies opting to instead start with either $VOPO_4$ or $LiVOPO_4$ as a precursor.[15,53]

As with $LiVOPO_4$, $NaVOPO_4$ has 3 polymorphs, which are closely related to their Li analogs and share the same naming systems. The major difference is that the ε polymorph of $NaVOPO_4$ has a monoclinic structure, due to it only having a single Na-site, compared to $LiVOPO_4$ which is triclinic and has two Li-sites. However, the two structures have very similar $VOPO_4$ framework.

Lin et al. predicted that the ε polymorph is the most stable, followed by the α_I and β polymorphs which have similar thermodynamic stabilities. Experimentally, the ε polymorph has been synthesized using a variety of methods, including SS and SG.[52] On the other hand, the α_I and β polymorphs have only been synthesized by reacting α_I-[54a,b] or β-$VOPO_4$[15,53c] with a Na-source. The $VOPO_4$ can either be synthesized directly or by delithiating $LiVOPO_4$.

Lin et al. have also predicted the voltage profiles of each $NaVOPO_4$ polymorph. A comparison of the calculated profiles with profiles from various studies is shown in **Figure 17**. The calculations show that the voltage profiles of $NaVOPO_4$ would be 0.3–0.6 V lower than those of $LiVOPO_4$, which fits the expectations for most Na-ion cells.[54] They also predict that the voltage at which the insertion of the 1st Na^+ ion would be highest is in the ε polymorph, followed by the α_I then the β polymorphs. This generally fits experimental data, with the exception of the data from Fang et al., which shows a higher voltage than expected.

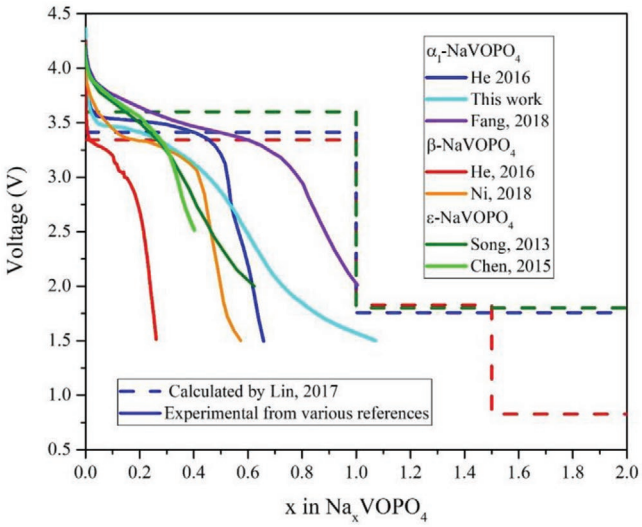

Figure 17. Comparison of calculated and experimental voltage profiles from various references.[15,52,-53]

Lin et al. calculated that the bandgaps and diffusion barriers of $NaVOPO_4$ are less beneficial for the electronic and ionic transport than those of $LiVOPO_4$. This implies that $NaVOPO_4$ will need particle-size reduction and conductive carbon coating in order to become electrochemically active. This fits with all the experimental data, which all require HEBM and some form of carbon additive in order to improve the capacity. Even utilizing these methods, no study has attained even full 1 Na cycling within the voltage range of 2.5–4.5 V. Thus, plenty of optimization is still needed. Lin et al. also predict that the α_I polymorph would perform the best out of all the polymorphs, due to its lower diffusion barriers. This fits with the experimental data in literature, which show that the α_I polymorph has the highest capacity among the various polymorphs.

Lin et al. also predicted the voltage profiles for the insertion of the 2nd Na^+ ion. However, this insertion has not been observed experimentally in these three $NaVOPO_4$ phases. This is possibly due to defects introduced by HEBM or a need to explore a lower voltage window in order to observe this insertion reaction. There have also been no studies on the chemical sodiation of (Na)$VOPO_4$ into Na_2VOPO_4. Such studies will be needed in order to better understand the electrochemical insertion of the 2nd Na^+ ion.

8. $KVPO_4(O,F)$ and NH_4VOPO_4 as Open Structures for Cycling Larger Cations

Synthesis of several $AVOPO_4$ compounds were reported, where A = K, Rb, Cs, and NH_4^+, some via direct synthesis and others by insertion into a $VOPO_4$ precursor.[55] The presence of larger cations within the compound expands the unit cell volume, allowing ease of diffusion during electrochemical cycling of larger cations such as Na^+ and K^+.

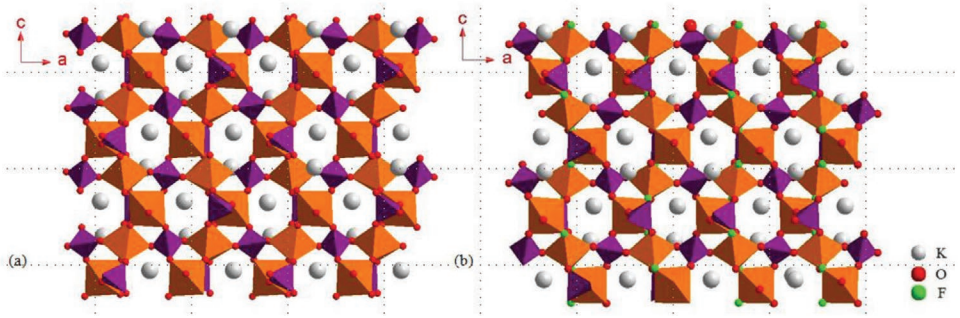

Figure 18. a) Crystal structure of $KVOPO_4$, and b) crystal structure of $KVPO_4F$.

Among the $AVOPO_4$ compounds, $KVOPO_4$ (**Figure 18**) has gained attention due to its structural similarity to $KTiOPO_4$, which is a widely studied compound due to its optical properties.[56] The synthesis of $KVOPO_4$ was first reported by Phillips et al. by hydrothermal method at 700 °C and 2.4 kbar.[55b] The resultant pure compound was characterized to be isostructural to $KTiOPO_4$ and denoted as α-$KVOPO_4$. The replacement of Ti with V results in an orthorhombic structure composed of single rows of corner sharing distorted VO_6 octahedra, linked together by PO_4 tetrahedra with space group $Pna2_1$ and a unit cell volume of 864.2 Å^3. α- $KVOPO_4$ and its fluorinated analog $KVPO_4F$ have been studied as cathodes in K-ion batteries by Chihara et al. with 1 M KPF_6/EC:PC electrolyte in a 2.0–5.0V versus K/K^+ window.[57] In α-$KVOPO_4$, the reaction before 4.45 versus K/K^+ was ascribed to a solid solution mechanism and the reaction between 4.45 and 5.0 versus K/K^+ to a two-phase mechanism based on in situ XRD data, where the new phase belongs to the same space group with different lattice parameters. The charging maximum extracted 0.63 K^+ per formula unit and resulted in a 3.3% volume change in unit cell. Reversible capacity of 84 mAhg^{-1} was obtained as a result of the reintercalation of K^+ into the 0.63 K^+ vacancies.

The fluorine compound, $KVPO_4F$, shares the same crystalline structure (space group Pna21) with $KVOPO_4$ (Figure 18). Fluorine atoms substitute the joint oxygen atoms between VO_6 octahedrons in the $[VO_5]_\infty$ chains, as shown in **Figure 19**a. According to the present literature and our own results, the unit cell volume of the $KVPO_4F$ is typically ≈1.5% larger than that of $KVOPO_4$, which may be due to the expanded VO_4F_2 octahedron.[11,58] The valence state of vanadium reduces to 3+ to balance the charge change by fluorine substitution (Figure 19b).

Researchers have cycled the $KVPO_4F$ phase in batteries using the V^{3+}/V^{4+} redox couple.[57,58] As shown in **Figure 20**a, the V^{3+}/V^{4+} redox exhibits a voltage of around 4 V versus Li/Li^+. This high voltage is largely resulted from the strong inductive effect of fluorine. Fedotov et al. extracted a maximum 0.83 K^+ per formula unit by charging the $KVPO_4F$ phase up to 5.0 V versus Li/Li^+ followed by a continuous holding for 48 h.[58] Based on the selected area electron diffraction (SAED) and electron diffraction tomography (EDT) data, they claimed that the charged phase becomes centrosymmetric belonging to the Pnan space group. The most K^+ deficient phase can reversibly store 0.7 Li^+ during the discharge corresponding to a capacity of ca. 110 mAhg^{-1}. Instead of following the initial K(1), K(2) sites, the Li^+ shares only partial K(2) sites and creates new Li(3) sites. The same group also studied diffusion of Li^+, Na^+, and K^+ in $KVPO_4F$ and reported highest apparent diffusion coefficient for K^+ ion.[59] Moreover, they have reported a novel $RbVOPO_4$ phase, which also adopts the $KTiOPO_4$ structure and is capable of Rb^+ and K^+ ion cycling.[60]

Chihara at al. also attempted to electrochemically extract potassium ions from $KVPO_4F$ but in a potassium cell (Figure 20b).[57] They observed a solid solution reaction upon K extraction from the in situ XRD data. Maximum 0.7 K^+ per formula unit can be extracted by charging up to 5.0 V versus K/K^+. Different from the lithium storage in the Li cell, Chihara et al. observed that the K^+ are fully accommodated in the initial K(1) and K(2) sites, resulting in a total structure reversibility upon cycling. The different behavior of Li^+ and K^+ intercalation in the K^+ deficiency polyhedron framework may be highly related to the size of the ions. Use of anode other than metallic potassium results in better cycling stability of K^+ cycling in $KVPO_4F$.[61]

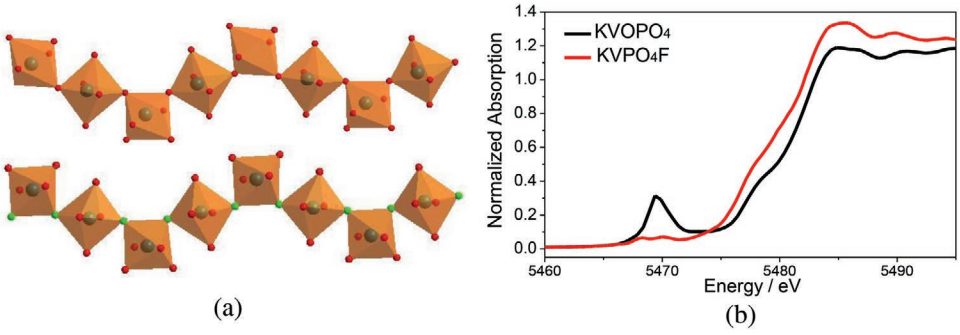

Figure 19. a) The $[VO_5]_\infty$ chains in $KVOPO_4$ and $KVPO_4F$. b) The XANES of $KVOPO_4$ and $KVPO_4F$.

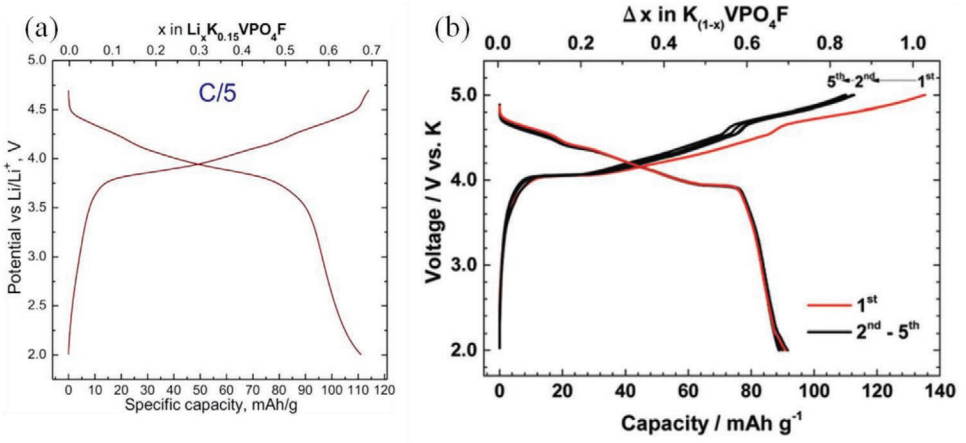

Figure 20. The voltage profiles of $KVPO_4F$ materials in Li a) and K b) cells.[57,58] Plot (a) reproduced with permission.[58] Copyright 2016, The American Chemical Society. Plot (b) reproduced with permission.[57] Copyright 2017, The Royal Society of Chemistry.

Similar to the lithium vanadyl phosphate ($LiVOPO_4$) and lithium vanadium fluorophosphates ($LiVPO_4F$),[62] it is also feasible to achieve multielectron reaction by taking advantage of the $V^{3+}\leftrightarrow V^{5+}$ and $V^{2+}\leftrightarrow V^{4+}$ redox couples for $KVOPO_4$ and $KVPO_4F$, respectively. As shown in **Figure 21**a, the $K_{0.15}VPO_4F$ structure can store multiple lithium ions in a voltage window of 1.5–4.7 V versus Li/Li^+. There are two distinct capacity regions at the high voltage of ≈3.8 V (V^{4+}/V^{3+}) and low voltage of ≈1.8 V (V^{3+}/V^{2+}).[63] The K-pillared polyhedron framework with large cavities can also accommodate more than one Na^+. As shown in Figure 21b, our results show that a K^+ deficient framework $K_{0.36}VOPO_4$ can deliver 235 $mAhg^{-1}$ discharge capacity in a sodium cell corresponding to 1.76 Na^+ per formula unit. Interestingly, the average voltages of the V^{5+}/V^{4+} and V^{4+}/V^{3+} for $K_{3.6}Na_xVOPO_4$ are similar to those of V^{4+}/V^{3+} and V^{3+}/V^{2+} for $K_{0.17}Na_xVPO_4F$. This analogy in voltages is a synergetic result of the fluorine introduction and potential difference between lithium and sodium metal. It is worthwhile to mention that the multiple sodium storage behavior have never been seen in other vanadyl phosphates members. We believe that the more open polyhedron framework of $KVOPO_4$ provides accessible room for the second Na, which can active the V^{4+}/V^{3+} in the vanadyl phosphate structure. The additional Na accommodation can extend the gravimetric energy density to a very high level of 600 $Whkg^{-1}$. But still, the voltage gap between the two active redox regions and the low voltage of the V^{3+}/V^{4+} redox remain challenging.

Later, another $KVOPO_4$ structure was discovered by Berrah et al. with much smaller unit cell belonging to $P2_12_12_1$ space group (named β-$KVOPO_4$)[64] and compared to the other $AVOPO_4$ with A = Li, K, Rb, Cs, NH_4. The β-$KVOPO_4$ is synthesized hydrothermally by an addition of a tungsten source which was noted to be essential for monophasic product formation. The powder XRD analysis of the β-$KVOPO_4$ indicates an orthorhombic structure with $P2_12_12_1$ space group and 467.9 $Å^3$ cell volume.[64] This phase is similar to the previously reported $RbVOPO_4$ and $CsVOPO_4$ frameworks which are built up of discrete VO_5 square pyramids linked by PO_4 octahedra.[55c] While the three compounds crystallize in the same space group, there are notable distortions that result from the difference in intercalated ion sizes. Berrah et al. argue that potassium is a "boundary cation" due to its ability to coordinate both in pyramidal and octahedral vanadyl monophosphates. The smaller cations such as Li^+ and Na^+ are strictly observed in structures with VO_6 chains. Potassium can exist both in octahedral vanadyl monophosphates such as α- $KVOPO_4$ as well as in the pyramidal β-phase. A layered $KVOPO_4{\cdot}nH_2O$ phase was obtained by potassiation and partial water removal from $K_{0.5}VOPO_4{\cdot}aH_2O$,

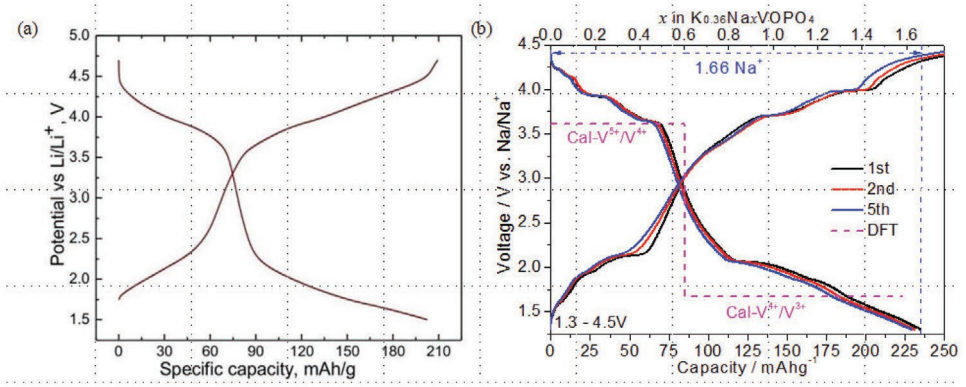

Figure 21. The multielectron behavior of $KVPO_4F$ in Li cell a), and $KVOPO_4$ in Na cell b).[63] Reproduced with permission.[63] Copyright 2018, WILEY.

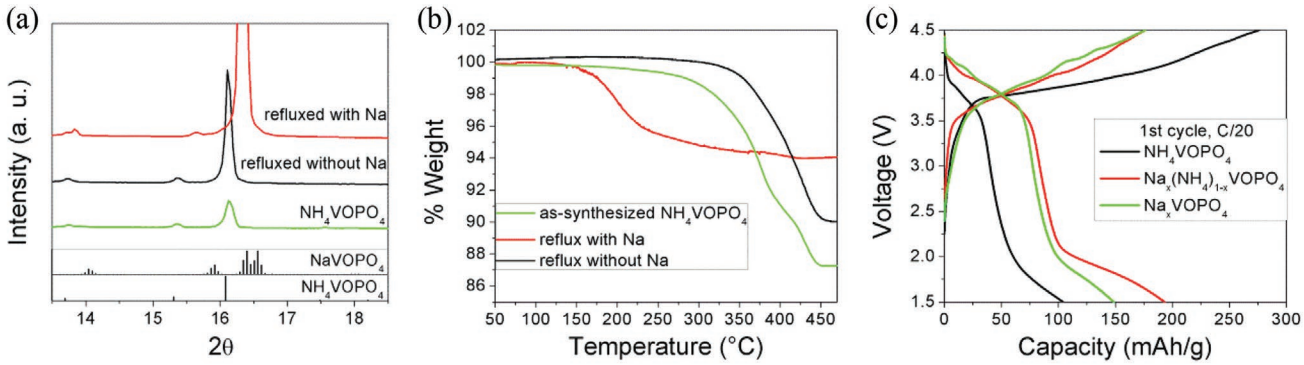

Figure 22. Comparison of reflux products a) peak shifts in XRD pattern b) TGA of the reflux products with and without NaBr source, c) Comparison of 1st cycle electrochemical performance of synthesized NH_4VOPO_4, $Na_x(NH_4)_{1-x}VOPO_4$, and Na_xVOPO_4 cycled in Na-ion cells between 1.5 and 4.5 V at C/20, where C is 2 Na.

and was shown to provide 115 mAh g^{-1} (0.2 C, average voltage 3.65 V).[65] Further comparison of $KVPO_4(O,F)$ phases with other cathode materials for potassium-ion batteries can be found in recent reviews.[66]

Interestingly, although being a larger cation than K^+, ammonia containing NH_4VOPO_4 is also built up of corner sharing VO_6 octahedra. This structure is highly similar to α-$KVOPO_4$ and has gained attention due to its highly porous $VOPO_4$ framework. It is possible to address the limitations of cation removal in $KVOPO_4$ phases by the use of this isostructural polymorph where instead of potassium, the $VOPO_4$ framework is pillared by the NH_4^+ which is a volatile cation. NH_4VOPO_4 has a very similar $VOPO_4$ framework to that of $KVOPO_4$ where the VO_6 chains are linked in alternating cis- and trans-configuration and joined together by PO_4 tetrahedra in a noncentrosymmetric framework. Due to the greater radii of NH_4^+ cations (Shannon radii of K^+ = 1.38 Å, NH_4^+ = 1.48 Å),[50] there is a larger distortion in ordering of the cations in the ammonium containing compound. In NH_4VOPO_4, cations are in zig-zag arrangement, whereas $KVOPO_4$ maintains linear ordering of K^+ ions. The hydrothermal synthesis of this compound was originally reported by Haushalter et al. although pure phase product was not achieved.[67] An interesting study done by Schindler et al. investigated the effect of synthesis conditions on formation of various microporous ammonium vanadyl phosphate compounds.[68] By altering the pH of solutions, different phases of $AVOPO_4$ (A = K^+ or NH_4^+) and their hydrate compounds were obtained. The hydrothermal synthesis of NH_4VOPO_4 was achieved by the use of V:P:(tEA):H_2O ratio of (1:4:(3.5):700 within a pH of 4.2–8.7. We have employed the molar ratio suggested by Schindler et al. in synthesizing the NH_4VOPO_4 phase and used V_2O_5 and $(NH_4)_2HPO_4$ as V and P sources. Also, 15% of water solvent was replaced by 100% ethanol in order to enhance the reducing environment for product formation. The solution was heated at 200 °C for 72 h and resultant product was filtered and dried in a 60 °C oven. The powder XRD analysis of the product indicates that this structure has orthorhombic symmetry with Pnn2 space group and lattice parameters of a = 10.511, b = 12.917, and c = 6.462 Å.[69]

Using TGA-MS in N_2 and O_2 with subsequent X-ray diffraction of the products we have shown that it is not possible to remove NH_4^+ from NH_4VOPO_4 without a phase change. Heating in O_2 versus N_2 indicate that removal of NH_4^+ requires ambient oxygen presence for structural stability. The heating in nitrogen product was identified to be $(VO)_2P_2O_7$, indicating stripping of structural oxygen during NH_4^+ removal. The XRD analysis of the samples heated in O_2 show a loss of crystallinity at 400 °C and the emergence of an unknown phase at 500 °C, followed by formation of γ-$VOPO_4$ at 700 °C. On the other hand, samples annealed in air form pure phase δ-$VOPO_4$ with a small amount of ε-$VOPO_4$ which later form pure phase β-$VOPO_4$ following the removal of NH_4^+ around 400 °C. Therefore, NH_4^+ can be removed thermally, however, the desired porous $VOPO_4$ phase is not stable without the presence of pillaring NH_4^+ ions.

In order to stabilize the structure before completely removing the ammonium ions, substitution of some of the NH_4^+ with Na^+ was used to pillar the framework. Refluxing NH_4VOPO_4 in 3 M NaBr in tetraethylene glycol solution successfully substitutes Na^+ with NH_4^+ while maintaining structural integrity. **Figure 22**a shows the XRD peak shifts in the reflux products with Na source, while Figure 21b shows TGA graphs with decreased weight loss, confirming Na substitution. The ICP-MS analysis of the reflux product indicates the presence of 0.82 Na per $VOPO_4$ unit. The electrochemical tests in Na-ion cells were performed for the NH_4VOPO_4, $Na_x(NH_4)_{1-x}VOPO_4$ and Na_xVOPO_4 which was obtained by annealing the reflux sample (Figure 21c). Following the first discharge cycle, capacities of 193, 148, and 104 mAh g^{-1} for $Na_x(NH_4)_{1-x}VOPO_4$, $NaVOPO_4$, and NH_4VOPO_4 were obtained. Thus, substitution with Na^+ improves the electrochemical performance of NH_4VOPO_4, while complete removal of NH_4^+ worsens it. Presence of a small amount of NH_4^+ may be pillaring the structure during cycling of Na^+, preventing structural collapse, similar to the small amount of K^+ in K_xVOPO_4 upon Na cycling. Although theoretical capacity of 258 mAh g^{-1} (for 2 Na^+ cycling) was not achieved, we were able to illustrate the candidacy of this structure as a host for larger cation substitution.[69]

9. Conclusion

This review has demonstrated the capabilities of A_xVOPO_4 family as multielectron cathode materials for alkali metal batteries. We

have shown that it is possible to cycle two Li^+ ions for at least 50 cycles in ε-$VOPO_4$ using nanocrystals coated with graphene nanoplatelets. Also, multiple Na^+ ion cycling is possible in more open K_xVOPO_4 structure. However, the challenges of A_xVOPO_4 family originating from poor electronic and ionic conductivities, metastability of $x > 1$ phases and reactivity toward organic electrolytes still limit their high-rate and cycling performance. The questions to be addressed in the future work include further understanding and prevention of side reactions at both high and low voltages, in particular, understanding the role of protons in the hydrothermally synthesized materials and incorporated upon cycling. The approaches to increasing Coulombic efficiency and cycling stability of these materials may include further development of synthesis methods leading to well-crystalline nanoparticles; use of different electrolytes, i.e., ionic liquids and solid electrolytes, along with further work on surface coating and substitution.

Supporting Information

Supporting Information is available from the Wiley Online Library or from the author.

Acknowledgements

This work was supported as part of NECCES, an Energy Frontier Research Center funded by the U.S. Department of Energy, Office of Science, Office of Basic Energy Sciences under Award No. DE-SC0012583. This research used resources of the Advanced Photon Source, a U.S. Department of Energy (DOE) Office of Science User Facility operated for the DOE Office of Science by Argonne National Laboratory under Contract No. DE-AC02-06CH11357.

Conflict of Interest

The authors declare no conflict of interest.

Keywords

cathode materials, Li-ion batteries, vanadium compounds

Received: August 15, 2020
Revised: October 1, 2020
Published online:

[1] a) M. S. Whittingham, *Chem. Rev.* **2014**, *114*, 11414; b) C. Masquelier, L. Croguennec, *Chem. Rev.* **2013**, *113*, 6552; c) N. A. Chernova, M. Roppolo, A. C. Dillon, M. S. Whittingham, *J. Mater. Chem.* **2009**, *19*, 2526; d) X. M. Xu, F. Y. Xiong, J. S. Meng, X. P. Wang, C. J. Niu, Q. Y. An, L. Q. Mai, *Adv. Funct. Mater.* **2020**, *30*, 1904398; e) M. S. Whittingham, *Chem. Rev.* **2004**, *104*, 4271; f) M. S. Whittingham, Y. N. Song, S. Lutta, P. Y. Zavalij, N. A. Chernova, *J. Mater. Chem.* **2005**, *15*, 3362.

[2] P. Y. Zavalij, M. S. Whittingham, *Acta Crystallogr., Sect. B: Struct. Sci.* **1999**, *55*, 627.

[3] a) D. McNulty, D. N. Buckley, C. O'Dwyer, *J. Power Sources* **2014**, *267*, 831; b) P. Liu, K. Zhu, Y. Gao, H. Luo, L. Lu, *Adv. Energy Mater.* **2017**, *7*, 1700547; c) Y. Yue, H. Liang, *Adv. Energy Mater.* **2017**, *7*, 1602545; d) J. H. Yao, Y. W. Li, R. C. Masse, E. Uchaker, G. Z. Cao, *Energy Storage Mater.* **2018**, *11*, 205.

[4] B. Senthilkumar, C. Murugesan, L. Sharma, S. Lochab, P. Barpanda, *Small Methods* **2019**, *3*, 1800253.

[5] Y. Huang, Y. C. Lin, D. M. Jenkins, N. A. Chernova, Y. Chung, B. Radhakrishnan, I. H. Chu, J. Fang, Q. Wang, F. Omenya, S. P. Ong, M. S. Whittingham, *ACS Appl. Mater. Interfaces* **2016**, *8*, 7013.

[6] a) E. Bordes, *Catal. Today* **1987**, *1*, 499; b) G. F. Benabdelouahab, J. C. Volta, R. Olier, *J. Catal.* **1994**, *148*, 334; c) P. Amorós, M. D. Marcos, M. Roca, J. Alamo, A. Beltrán-Porter, D. Beltrán-Porter, *J. Phys. Chem. Solids* **2001**, *62*, 1393; d) S. C. Lim, J. T. Vaughey, W. T. A. Harrison, L. L. Dussack, A. J. Jacobson, J. W. Johnson, *Solid State Ionics* **1996**, *84*, 219.

[7] a) A. S. Hameed, M. Nagarathinam, M. V. Reddy, B. V. R. Chowdari, J. J. Vittal, *J. Mater. Chem.* **2012**, *22*, 7206; b) K. H. Lii, C. H. Li, C. Y. Cheng, S. L. Wang, *J. Solid State Chem.* **1991**, *95*, 352; c) A. V. Lavrov, V. P. Nikolaev, G. G. Sadikov, M. A. Poraikoshits, *Dokl. Akad. Nauk Sssr* **1982**, *266*, 343.

[8] a) T. A. Kerr, J. Gaubicher, L. F. Nazar, *Electrochem. Solid-State Lett.* **1999**, *3*, 460; b) Y. N. Song, P. Y. Zavalij, M. S. Whittingham, *J. Electrochem. Soc.* **2005**, *152*, A721.

[9] F. Girgsdies, W. S. Dong, J. K. Bartley, G. J. Hutchings, R. Schlögl, T. Ressler, *Solid State Sci.* **2006**, *8*, 807.

[10] a) M. Bianchini, J. M. Ateba-Mba, P. Dagault, E. Bogdan, D. Carlier, E. Suard, C. Masquelier, L. Croguennec, *J. Mater. Chem. A* **2014**, *2*, 10182; b) Z. H. Chen, Q. Y. Chen, L. Q. Chen, R. B. Zhang, H. Zhou, N. A. Chernova, M. S. Whittingham, *J. Electrochem. Soc.* **2013**, *160*, A1777.

[11] Y. C. Lin, M. F. V. Hidalgo, I. H. Chu, N. A. Chernova, M. S. Whittingham, S. P. Ong, *J. Mater. Chem. A* **2017**, *5*, 17421.

[12] N. F. Quackenbush, L. Wangoh, D. O. Scanlon, R. Zhang, Y. Chung, Z. Chen, B. Wen, Y. Lin, J. C. Woicik, N. A. Chernova, S. P. Ong, M. S. Whittingham, L. F. J. Piper, *Chem. Mater.* **2015**, *27*, 8211.

[13] C. Siu, I. D. Seymour, S. Britto, H. L. Zhang, J. Rana, J. Feng, F. O. Omenya, H. Zhou, N. A. Chernova, G. W. Zhou, C. P. Grey, L. F. J. Piper, M. S. Whittingham, *Chem. Commun.* **2018**, *54*, 7802.

[14] C. Ling, R. G. Zhang, F. Mizuno, *J. Mater. Chem. A* **2014**, *2*, 12330.

[15] G. He, A. Huq, W. H. Kan, A. Manthiram, *Chem. Mater.* **2016**, *28*, 1503.

[16] S. A. Hameed, M. Nagarathinam, M. V. Reddy, B. V. R. Chowdari, J. J. Vittal, *J. Mater. Chem.* **2012**, *22*, 7206.

[17] M. F. Hidalgo, Y. C. Lin, A. Grenier, D. D. Xiao, J. Rana, R. Tran, H. L. Xin, M. Zuba, J. Donohue, F. O. Omenya, I. H. Chu, Z. B. Wang, X. G. Li, N. A. Chernova, K. W. Chapman, G. W. Zhou, L. Piper, S. P. Ong, M. S. Whittingham, *J. Mater. Chem. A* **2019**, *7*, 8423.

[18] a) K. L. Harrison, C. A. Bridges, C. U. Segre, C. D. Varnado, D. Applestone, C. W. Bielawski, M. P. Paranthaman, A. Manthiram, *Chem. Mater.* **2014**, *26*, 3849; b) C. J. Allen, Q. Jia, C. N. Chinnasamy, S. Mukerjee, K. M. Abraham, *J. Electrochem. Soc.* **2011**, *158*, A1250; c) G. He, C. A. Bridges, A. Manthiram, *Chem. Mater.* **2015**, *27*, 6699; d) G. He, W. H. Kan, A. Manthiram, *Chem. Commun.* **2018**, *54*, 13224.

[19] Y. C. Lin, B. H. Wen, K. M. Wiaderek, S. Sallis, H. Liu, S. H. Lapidus, O. J. Borkiewicz, N. F. Quackenbush, N. A. Chernova, K. Karki, F. Omenya, P. J. Chupas, L. F. J. Piper, M. S. Whittingham, K. W. Chapman, S. P. Ong, *Chem. Mater.* **2016**, *28*, 1794.

[20] Y. Shi, H. Zhou, I. D. Seymour, S. Britto, J. Rana, L. W. Wangoh, Y. Q. Huang, Q. Y. Yin, P. J. Reeves, M. Zuba, Y. Chung, F. Omenya, N. A. Chernova, G. W. Zhou, L. F. J. Piper, C. P. Grey, M. S. Whittingham, *ACS Omega* **2018**, *3*, 7310.

[21] L. W. Wangoh, S. Sallis, K. M. Wiaderek, Y. C. Lin, B. H. Wen, N. F. Quackenbush, N. A. Chernova, J. H. Guo, L. Ma, T. P. Wu, T. L. Lee, C. Schlueter, S. P. Ong, K. W. Chapman, M. S. Whittingham, L. F. J. Piper, *Appl. Phys. Lett.* **2016**, *109*, 053904

[22] I. D. Seymour, *unpublished* **2020**.

[23] L. J. M. Davis, X. J. He, A. D. Bain, G. R. Goward, *Solid State Nucl. Magn. Reson.* **2012**, *42*, 26.
[24] M. M. Ren, Z. Zhou, X. P. Gao, *J. Appl. Electrochem.* **2010**, *40*, 209.
[25] S. Britto, I. D. Seymour, D. Halat, M. F. V. Hidalgo, C. Siu, P. J. Reeves, H. Zhou, N. A. Chernova, M. S. Whittingham, C. P. Grey, *J. Mater. Chem. A* **2020**, *8*, 5546.
[26] a) B. M. Azmi, T. Ishihara, H. Nishiguchi, Y. Takita, *Electrochemistry* **2003**, *71*, 1108; b) Y. Yang, H. S. Fang, J. Zheng, L. P. Li, G. S. Li, G. F. Yan, *Solid State Sci.* **2008**, *10*, 1292.
[27] a) A. Padhi, K. S. Nanjundaswamy, J. Goodenough, *J. Electrochem. Soc.* **1997**, *144*, 1188; b) M. Gaberscek, R. Dominko, J. Jamnik, *Electrochem. Commun.* **2007**, *9*, 2778.
[28] a) N. J. Yun, H.-W. Ha, K. H. Jeong, H.-Y. Park, K. Kim, *J. Power Sources* **2006**, *160*, 1361; b) C.-Z. Lu, G. T.-K. Fey, H.-M. Kao, *J. Power Sources* **2009**, *189*, 155.
[29] R. Malik, D. Burch, M. Bazant, G. Ceder, *Nano Lett.* **2010**, *10*, 4123.
[30] Y. Shi, H. Zhou, S. Britto, I. D. Seymour, K. M. Wiaderek, F. Omenya, N. A. Chernova, K. W. Chapman, C. P. Grey, M. S. Whittingham, *Electrochem. Commun.* **2019**, *105*, 106491
[31] a) K. L. Harrison, A. Manthiram, *Chem. Mater.* **2013**, *25*, 1751; b) M. M. Ren, Z. Zhou, X. P. Gao, L. Liu, W. X. Peng, *J. Phys. Chem. C* **2008**, *112*, 13043; c) K. Saravanan, H. S. Lee, M. Kuezma, J. J. Vittal, P. Balaya, *J. Mater. Chem.* **2011**, *21*, 10042; d) Y. M. Chung, E. Cassidy, K. Lee, C. Siu, Y. Q. Huang, F. Omenya, J. Rana, K. M. Wiaderek, N. A. Chernova, K. W. Chapman, L. F. J. Piper, M. S. Whittingham, *ACS Appl. Energy Mater.* **2019**, *2*, 4792.
[32] a) M. M. Ren, Z. Zhou, L. W. Su, X. P. Gao, *J. Power Sources* **2009**, *189*, 786; b) Z. G. Liu, Z. Su, H. L. Tian, *Int. J. Electrochem. Sci.* **2017**, *12*, 10107; c) A. P. Tang, Z. Q. He, J. Shen, G. R. Xu, *Adv. Chem. Res.* **2012**, *554-556*, 436; d) H. Zhou, Y. Shi, F. Xin, F. Omenya, M. S. Whittingham, *ACS Appl. Mater. Interfaces* **2017**, *9*, 28537; e) L. Wang, L. B. Yang, L. Gong, X. Q. Jiang, K. Yuan, Z. B. Hu, *Electrochim. Acta* **2011**, *56*, 6906; f) H. T. Kuo, N. C. Bagkar, R. S. Liu, C. H. Shen, D. S. Shy, X. K. Xing, J. F. Lee, J. M. Chen, *J. Phys. Chem. B* **2008**, *112*, 11250.
[33] a) J.-M. Ateba Mba, C. Masquelier, E. Suard, L. Croguennec, *Chem. Mater.* **2012**, *24*, 1223; b) J. M. A. Mba, L. Croguennec, N. I. Basir, J. Barker, C. Masquelier, *J. Electrochem. Soc.* **2012**, *159*, A1171.
[34] a) J. Barker, M. Y. Saidi, J. L. Swoyer, *J. Electrochem. Soc.* **2004**, *151*, A796; b) K. Nagamine, T. Honma, T. Komatsu, *J. Am. Ceram. Soc.* **2008**, *91*, 3920.
[35] C. Kaplan, M. F. V. Hidalgo, M. Zuba, N. A. Chernova, L. F. J. Piper, M. S. Whittingham, unpublished **2020**.
[36] L. L. Hench, J. K. West, *Chem. Rev.* **1990**, *90*, 33.
[37] B. M. Azmi, H. S. Munirah, T. Ishihara, Y. Takita, *Ionics* **2005**, *11*, 402.
[38] M. Oghbaei, O. Mirzaee, *J. Alloys Compd.* **2010**, *494*, 175.
[39] a) K. S. Park, J. T. Son, H. T. Chung, S. J. Kim, C. H. Lee, H. G. Kim, *Electrochem. Commun.* **2003**, *5*, 839; b) T. V. S. L. Satyavani, A. Srinivas Kumar, P. S. V. Subba Rao, *Int. J. Eng. Sci. Res. Technol.* **2016**, *19*, 178; c) L. Wang, Y. Huang, R. Jiang, D. Jia, *Electrochim. Acta* **2007**, *52*, 6778.
[40] J. Rana, Y. Shi, M. J. Zuba, K. M. Wiaderek, J. Feng, H. Zhou, J. Ding, T. P. Wu, G. Cibin, M. Balasubramanian, F. Omenya, N. A. Chernova, K. W. Chapman, M. S. Whittingham, L. F. J. Piper, *J. Mater. Chem. A* **2018**, *6*, 20669.
[41] a) K. Zaghib, A. Mauger, J. B. Goodenough, F. Gendron, C. M. Julien, *Chem. Mater.* **2007**, *19*, 3740; b) M. S. Islam, D. J. Driscoll, C. A. J. Fisher, P. R. Slater, *Chem. Mater.* **2005**, *17*, 5085.
[42] a) C. Delacourt, C. Wurm, L. Laffont, J. B. Leriche, C. Masquelier, *Solid State Ionics* **2006**, *177*, 333; b) T. Zhao, W. Xu, Q. Ye, J. Cheng, H. Zhao, Z. Wu, D. Xia, W. Chu, *J. Synchrotron Radiat.* **2010**, *17*, 584.
[43] a) J. Chen, M. J. Vacchio, S. Wang, N. Chernova, P. Y. Zavalij, M. S. Whittingham, *Solid State Ionics* **2008**, *178*, 1676; b) F. Omenya, N. A. Chernova, S. Upreti, P. Y. Zavalij, K.-W. Nam, X.-Q. Yang, M. S. Whittingham, *Chem. Mater.* **2011**, *23*, 4733; c) F. Omenya, N. A. Chernova, Q. Wang, R. Zhang, M. S. Whittingham, *Chem. Mater.* **2013**, *25*, 2691; d) F. Omenya, N. A. Chernova, R. Zhang, J. Fang, Y. Huang, F. Cohen, N. Dobrzynski, S. Senanayake, W. Xu, M. S. Whittingham, *Chem. Mater.* **2013**, *25*, 85; e) K. L. Harrison, C. A. Bridges, M. P. Paranthaman, C. U. Segre, J. Katsoudas, V. A. Maroni, J. C. Idrobo, J. B. Goodenough, A. Manthiram, *Chem. Mater.* **2013**, *25*, 768; f) N. Meethong, Y.-H. Kao, S. A. Speakman, Y.-M. Chiang, *Adv. Funct. Mater.* **2009**, *19*, 1060; g) M. Wagemaker, B. L. Ellis, D. Lützenkirchen-Hecht, F. M. Mulder, L. F. Nazar, *Chem. Mater.* **2008**, *20*, 6313.
[44] L. Z. Xiong, Y. G. Wang, Y. X. Wu, W. P. Liu, Z. Q. He, *Ionics* **2015**, *21*, 2471.
[45] M. A. Bustam, Z. Man, S. Maitra, T. Ishihara, *Trans. Indian Ceram. Soc.* **2013**, *72*, 108.
[46] a) G. Ladwig, *Z. Anorg. Allg. Chem.* **1965**, *338*, 266; b) L. Beneš, K. Richtrova, J. Votinský, J. Kalousová, V. Zima, *Powder Diffr.* **1993**, *8*, 130; c) G. Bagnasco, L. Beneš, P. Galli, M. A. Massucci, P. Patrono, M. Turco, V. Zima, *J. Therm. Anal. Calorim.* **1998**, *52*, 615; d) P. Ciambelli, L. Lisi, P. Patrono, G. Ruoppolo, G. Russo, *Catal. Lett.* **2002**, *82*, 243; e) F. Rouvet, J.-M. Herrmann, J.-C. Volta, *J. Chem. Soc., Faraday Trans.* **1994**, *90*, 1441; f) K. Melánová, J. Votinský, L. Beneš, V. Zima, *Mater. Res. Bull.* **1995**, *30*, 1115; g) S. Marengo, P. Patrono, P. Comotti, G. Galli, P. Galli, M. A. Massucci, M. T. Meloni, *Appl. Catal., A* **2002**, *230*, 219; h) S. Roy, L. Yeasmin, M. Rahman , *J. Bangladesh Acad. Sci.* **2019**, *43*, 31.
[47] a) D.-J. Park, R. Rajagopal, K.-S. Ryu, *J. Ind. Eng. Chem.* **2020**, *83*, 260; b) S. H. Lee, K. S. Ryu, *Bull. Korean Chem. Soc.* **2018**, *39*, 1266.
[48] a) B. H. Wen, Q. Wang, Y. Lin, N. A. Chernova, K. Karki, Y. Chung, F. Omenya, S. Sallis, L. F. J. Piper, S. P. Ong, M. S. Whittingham, *Chem. Mater.* **2016**, *28*, 3159; b) M. F. V. Hidalgo, I. Buyuker, G. E. Kamm, Z. Zhu, A. Grenier, M. Zuba, Z. Deng, Y. Zong, C. Kaplan, N. A. Chernova, G. Zhou, L. F. J. Piper, S. P. Ong, K. W. Chapman, M. S. Whittingham, *J. Mater. Chem. A* in preparation; c) K. Lee, *unpublished*; d) C. Siu, *unpublished*.
[49] K. T. Jacob, S. Raj, L. Rannesh, *Int. J. Mater. Res.* **2007**, *98*, 776.
[50] R. D. Shannon, *Acta Crystallogr. A* **1976**, *32*, 751.
[51] a) S. Patoux, C. Masquelier, *Chem. Mater.* **2002**, *14*, 5057; b) H. Morimoto, D. Ito, Y. Ogata, T. Suzuki, K. Sakamaki, T. Tsuji, M. Hirukawa, A. Matsumoto, S.-i. Tobishima, *Electrochemistry* **2016**, *84*, 878.
[52] a) J. Song, M. Xu, L. Wang, J. B. Goodenough, *Chem. Commun.* **2013**, *49*, 5280; b) C.-Y. Chen, K. Matsumoto, T. Nohira, R. Hagiwara, *J. Electrochem. Soc.* **2015**, *162*, A2093.
[53] a) Y. Fang, Q. Liu, L. Xiao, Y. Rong, Y. Liu, Z. Chen, X. Ai, Y. Cao, H. Yang, J. Xie, C. Sun, X. Zhang, B. Aoun, X. Xing, X. Xiao, Y. Ren, *Chem* **2018**, *4*, 1167; b) G. He, W. H. Kan, A. Manthiram, *Chem. Mater.* **2016**, *28*, 682; c) Y. Ni, G. He, *Electrochim. Acta* **2018**, *292*, 47.
[54] S. P. Ong, V. L. Chevrier, G. Hautier, A. Jain, C. Moore, S. Kim, X. Ma, G. Ceder, *Energy Environ. Sci.* **2011**, *4*, 3680.
[55] a) C. J. O'Connor, V. Soghomonian, R. C. Haushalter, Z. Wang, J. Zubieta, *J. Appl. Phys.* **1994**, *75*, 5859; b) M. L. F. Phillips, W. T. A. Harrison, T. E. Gier, G. D. Stucky, G. V. Kulkarni, J. K. Burdett, *Inorg. Chem.* **1990**, *29*, 2158; c) K.-H. Lii, W.-C. Liu, *J. Solid State Chem.* **1993**, *103*, 38.
[56] P. I. Tordjman, E. Masse, J. C. Guitel, *Z. Kristallogr.– Cryst. Mater.* **1974**, *139*, 103.
[57] K. Chihara, A. Katogi, K. Kubota, S. Komaba, *Chem. Commun.* **2017**, *53*, 5208.
[58] S. S. Fedotov, N. R. Khasanova, A. S. Samarin, O. A. Drozhzhin, D. Batuk, O. M. Karakulina, J. Hadermann, A. M. Abakumov, E. V. Antipov, *Chem. Mater.* **2016**, *28*, 411.
[59] V. A. Nikitina, S. S. Fedotov, S. Yu. Vassiliev, A. Sh. Samarin, N. R. Khasanova, E. V. Antipov, *J. Electrochem. Soc.* **2017**, *164*, A6373.

[60] S. S. Fedotov, A. S. Samarin, V. A. Nikitina, D. A. Aksyonov, S. A. Sokolov, A. Zhugayevych, K. J. Stevenson, N. R. Khasanova, A. M. Abakumov, E. V. Antipov, *J. Mater. Chem. A* **2018**, *6*, 14420.
[61] J. Y. Liao, Q. Hu, X. D. He, J. X. Mu, J. R. Wang, C. H. Chen, *J. Power Sources* **2020**, *451*, 227739.
[62] J. Barker, M. Y. Saidi, J. L. Swoyer, *J. Electrochem. Soc.* **2003**, *150*, A1394.
[63] J. Ding, Y. C. Lin, J. Liu, J. Rana, H. L. Zhang, H. Zhou, I. H. Chu, K. M. Wiaderek, F. Omenya, N. A. Chernova, K. W. Chapman, L. F. J. Piper, S. P. Ong, M. S. Whittingham, *Adv. Energy Mater.* **2018**, *8*, 1800221.
[64] F. Berrah, A. Guesdon, A. Leclaire, M.-M. Borel, J. Provost, B. Raveau, *Solid State Sci.* **2001**, *3*, 477.
[65] J. Y. Liao, Q. Hu, B. Che, X. Ding, F. Chen, C. H. Chen, *J. Mater. Chem. A* **2019**, *7*, 15244.
[66] a) X. Zhang, D. Yang, X. Rui, Y. Yu, S. Huang, *Curr. Opin. Electrochem.* **2019**, *18*, 24; b) T. Hosaka, K. Kubota, A. S. Hameed, S. Komaba, *Chem. Rev.* **2020**, *120*, 6358.
[67] R. C. Haushalter, Q. Chen, V. Soghomonian, J. Zubieta, C. J. O'Connor, *J. Solid State Chem.* **1994**, *108*, 128.
[68] M. Schindler, W. Joswig, W. H. Baur, *J. Solid State Chem.* **1997**, *134*, 286.
[69] I. Buyuker, *unpublished*.

Natasha A. Chernova received her B.S. (1996) and M.S. (1998) in Materials Science, and her Ph.D. (2001) in Physics from M. V. Lomonosov Moscow State University, Russia. She received a one-year fellowship from Corning Inc. in 2001 to work with Prof. Eric Cotts at Binghamton University on microcalorimetry and thermodynamics of metals and alloys. She joined Prof. M. Stanley Whittingham's group in 2002, where she studies transition metal oxides and phosphates as electrode materials for lithium ion batteries, with focus on structure, reaction mechanism, and magnetic properties as a complementary tool for structural characterization.

Marc Francis V. Hidalgo received his B.S. in Chemistry (2014) and Materials Science and Engineering (2015) from the Ateneo de Manila University in the Philippines, where he worked on low-cost instrumentation and next-generation solar cells. He received the USAID-STRIDE scholarship to pursue a Professional Science Masters degree, which combines both Materials S&E and business training, under the mentorship of Dr. Whittingham in the US. He remained for Ph.D. in Materials, completed in 2020, working on next-generation Li-ion battery materials. Back in the Philippines, he continues to work on renewables, with a focus on solar paired with energy storage for grid-based applications.

Kamila M. Wiaderek is a chemist within the X-ray Science Division at Advanced Photon Source, Argonne National Laboratory where she leads electrochemistry laboratory and supports user programs focused on energy storage. She applies synchrotron-based characterization techniques (pair distribution function, diffraction, and small angle scattering) to understand structure–function relationships in battery materials. She received her B.S./M.S. (2003) in Mineralogy and Geochemistry from AGH University of Science and Technology Krakow, Poland and her Ph.D. in electrochemistry (2011) from Miami University, Oxford Ohio USA with James A. Cox. She joined Argonne as a post-doctoral scholar in 2011 and became staff in 2015.

Shyue Ping Ong is an associate professor in the Department of NanoEngineering at the University of California, San Diego. He leads the Materials Virtual Lab, a research group focused on the interdisciplinary application of high-throughput first-principles computations and machine learning to the study and design of materials. He received his B.A. and M.Eng. from Cambridge University and Ph.D. in materials science and engineering at Massachusetts Institute of Technology in 2011.

Clare P. Grey is the Geoffrey-Moorhouse-Gibson and Royal Society Professor of Chemistry at Cambridge University. After receiving a B.A. and D. Phil. from Oxford University, she was a post-doctoral fellow at Nijmegen and at DuPont CR&D. She joined Stony Brook University in 1994, moving to Cambridge in 2009, maintaining an adjunct Professorship at Stony Brook. She is a fellow of the Royal Society and a foreign member of the American Academy of Arts and Sciences. Her current research interests include the use of solid-state NMR and diffraction-based methods to determine structure-function relationships in materials for energy storage and conversion.

M. Stanley Whittingham is the 2019 Chemistry Nobel Laureate and Distinguished Professor of Chemistry and Materials at Binghamton University (SUNY). After receiving a B.A. and D. Phil. from Oxford University in solid-state chemistry he was a post-doctoral fellow in Materials S&E at Stanford University, following which he joined the Corporate Research Laboratory of Exxon. It was there that he and his colleagues made the discoveries that led to the Li-ion battery. In 1988, he returned to academia at Binghamton, where he has continued his research on materials for energy applications. He has the led the DOE NECCES EFRC since 2014.